GeoStorage

Vol. 1, No. 2, p. 137-157, 2025

Review article

Advancements in Pore-Scale Imaging of CO_2 Desiccation Dynamics: A Review of Experimental Method for Deep Saline Aquifer Storage Systems

Jie Ren[1,2], Zhipeng Gao[1], Yuan Wang[1,2]*

[1] *Hohai University, 1 Xikang Road, Nanjing 210024, China*
[2] *The National Key Laboratory of Water Disaster Prevention, 1 Xikang Road, Nanjing 210024, China*

Keywords:
Microscopic
porous media
salt precipitation
visualization
dry-out

Cited as:
Ren J, Gao ZP, Wang Y. 2025. Advancements in Pore-Scale Imaging of CO_2 Desiccation Dynamics: A Review of Experimental Method for Deep Saline Aquifer Storage Systems. *GeoStorage*, 1(2), 137-157.
https://doi.org/10.46690/gs.2025.02.04

Abstract:
Against the backdrop of global carbon neutrality goals, injecting CO_2 into deep saline aquifers has become a critical engineering strategy for large-scale carbon storage. However, salt precipitation during injection poses significant challenges, causing pore clogging and permeability reduction that threaten to the long-term safety and efficacy of CO_2 storage. Therefore, an in-depth investigation into the mechanisms and influencing factors of salt precipitation under gas-brine multiphase flow conditions is essential for ensuring the stable operation of CO_2 sequestration projects in deep saline aquifers. This paper comprehensively reviews recent applications of micro visualization techniques to investigate the dry-out effect during gas injection. It first addresses the visualization of interfacial stability and the complete drying process during displacement, followed by a discussion of experimental results from the literature focusing on key factors such as boundary conditions, salinity, and pore characteristics. High-salinity conditions were observed to intensify salt precipitation and clogging risks. Furthermore, variations in injection rates, gas-liquid alternation strategies, and solution replenishment modes significantly influenced the location and extent of salt precipitation, resulting in variable impacts on permeability and injection efficiency.

1 Introduction

Global economic growth has driven a persistent increase in greenhouse gas emissions, particularly CO_2, thereby accelerating global warming. As of 2023, 124 countries have announced to net-zero targets. Major economies, such as the European Union, the United States, the United Kingdom, Canada, Japan, New Zealand, and South Africa, have pledged to achieve carbon neutrality by 2050 (Wei et al., 2022). China formally pledged in September 2020 to peak its carbon emissions by 2030 and achieve carbon neutrality by 2060 (Zhu et al., 2024). Carbon Capture and Storage (CCS) is recognized as a critical technology for mitigating CO_2 emissions and achieving net-zero targets (Cai et al., 2021). Due to their favorable reservoir characteristics, substantial storage capacity, economic feasibility, and long-term stability, deep saline aquifers are regarded as highly promising geological formations for large-scale carbon sequestration (Liu et al., 2016a; Leung et al., 2014). The global CCS project portfolio comprises 628 cumulative initiatives, 50 of which are currently in operation. Prominent operational examples utilizing deep saline formations include Norway's Snøhvit Project, Canada's Quest Facility, the Illinois Basin Decatur Project (U.S.), Qatar Energy's LNG CCS Complex, and Australia's Gorgon Carbon Dioxide Injection Project. Most forthcoming projects are also planned for deep saline aquifers (see Fig.1).

Deep saline aquifers are characterized by high salinity, where complex gas-brine interactions often induce extensive salt precipitation near the injection well. This phenomenon, known as the dry-out effect, occurs when actively injected CO_2 is driven

Yandy Scientific Press

* Corresponding author.
E-mail address: rj@hhu.edu.cn (Ren J); zhpgao11@163.com (Gao ZP); wangyuan@hhu.edu.cn (Wang Y)

Received Oct. 12, 2025; revised Nov. 08, 2025; accepted Nov. 12, 2025; available online Nov. 16, 2025.

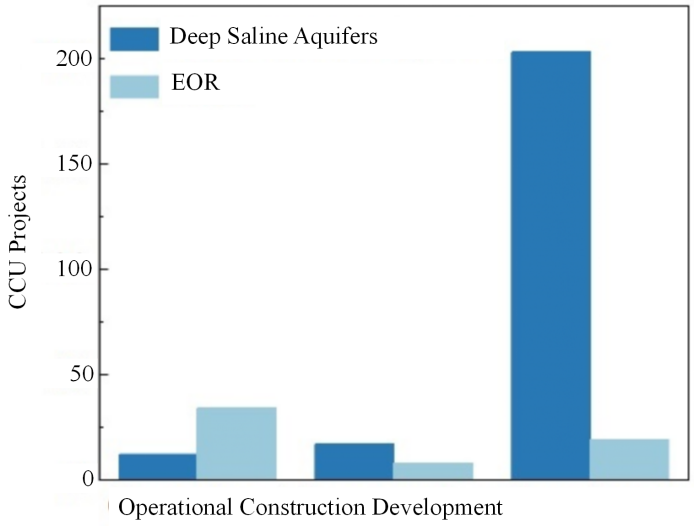

Fig. 1 Global distribution of CCS projects: comparing applications in deep saline aquifers versus enhanced oil recovery

by pressure gradients and velocity contrasts to displace and remove brine from the pore space of the saline aquifer, thereby altering local phase distributions and promoting salt precipitation (Wang and Liu, 2014). It substantially impairs injectivity and storage efficiency, while also escalating operational costs and heightening safety risks (Patil et al., 2020; Lopez et al., 2020; Kumar et al., 2020). For instance, salt precipitation has caused significant pressure build-up and injection impairment in CO_2 injection wells at the Ketzin pilot site in Germany (Baumann et al., 2014) and the Snøhvit project in Norway (Grude et al., 2014). Similar dry-out phenomena occur in other porous media systems, including soil salinization (Dong et al., 2021), oil and gas extraction (Zhou et al., 2021), and compressed air energy storage (Mouli-Castillo et al., 2019).

During CO_2 displacement in deep saline aquifers, the intricate coupling between flow dynamics and fluid properties introduces significant uncertainty in predicting the distribution and kinetics of salt crystallization (Cui et al., 2023). A comprehensive understanding of the crystallization mechanism is therefore crucial for optimizing reservoir management and enhancing storage efficiency. Both laboratory experiments and numerical simulations have confirmed that salt precipitation significantly alters the porosity and permeability of porous media (Ren et al., 2018). This process involves complex gas-brine two-phase flow, which is governed by a series of physicochemical interactions. The mutual dissolution of CO_2 and brine induces brine phase transitions, ultimately leading to salt precipitation. This crystallization modifies the aquifer's pore structure, thereby influencing CO_2-brine flow characteristics. Conversely, variations in CO_2-brine flow patterns further affect the formation and distribution of salt crystals, creating a complex feedback loop (Ren et al., 2018). Accurately capturing the dynamic evolution of this feedback loop in geological storage remains a formidable challenge. Existing simulation methods struggle to provide accuracy and multi-scale quantitative predictions (Ren et al., 2021).

Conventional core-flooding experimental apparatuses often fails to capture the kineties of salt precipitation within pore space during gas-brine two-phase flow (Akindipe et al., 2022). Challenges such as difficulty in refractive index matching, irreproducible pore structures, and poor experimental repeatability have limited the widespread adoption of transparent soil models for studying salt precipitation in deep saline aquifers (Zhang et al., 2022). Consequently, microfluidic visualization techniques have emerged as a powerful alternative, enabling real-time, high-resolution imaging of pore scale dynamics (Dąbrowski et al., 2025; Zou et al., 2024; Miri et al., 2015; He et al., 2019a; Naillon et al., 2017; Zhang et al., 2024; He et al., 2024; Yan et al., 2025; Zhou et al., 2022). This approach allows for precise micromodel design to simulate fluid migration and interfacial behavior in porous media (Dąbrowski et al., 2025; Zou et al., 2024). Researchers have thus employed these visualization techniques to investigate salt precipitation during two-phase flow, yielding critical insights into its formation mechanisms (Miri et al., 2015), spatial distribution patterns (He et al., 2019b), and dynamic evolution (Naillon et al., 2017).

Given the substantial impact of the dry-out effect on the safety and efficiency of geological CO_2 storage, alongside the unique capability of micro visualization techniques to elucidate multiphase flow in porous media, this paper systematically reviews and synthesizes applications and findings of these technologies in dry-out effect research. First, representative studies utilizing micro visualization to investigate interfacial stability are compared and synthesized, with a focus on mechanisms governing the interaction between evolving interfacial morphology and multiphase flow. Next, the review examines visualization-based studies of the entire drying process. Finally, it comprehensively reviews key factors controlling the dry-out effect, including salinity, boundary conditions, and pore characteristics, and summarizes the underlying mechanisms through which these factors influence dry-out dynamics. This

review aims to provide insights for further research on salt precipitation mechanisms and the optimization of geological storage strategies, while also offering a reference for studying salt precipitation in porous media across other disciplines.

2 Micro visualization systems and chip fabrication technology

Micro visualization is an experimental technology designed for precise observation and dynamic monitoring of fluid behavior at the pore scale. It has become a key methodology for investigating fluid migration and salt precipitation in porous media. The fundamental principle involves the use of high-resolution microscopic imaging within a controlled experimental system to capture intricate details of complex multiphase flow behavior and interfacial evolution. A typical micro visualization system comprises three core components: a fluid delivery system, an observation system, and a data acquisition system (Fig.2). The fluid delivery system enables precise control over injection rates and flow conditions. The observation system, which typically integrates optical or fluorescence microscopy with high-speed cameras, captures transient flow dynamics and interfacial changes at the pore scale. The data acquisition system records experimental processes in real time, collecting high-resolution images, video data, and relevant experimental parameters.

Common materials for fabricating micro visualization chips include silicon wafers, glass, and polymers such as polydimethylsiloxane (PDMS). Among these, silicon wafers serve as a fundamental material for microfluidic chips owing to their exceptional physical and chemical properties. Their high mechanical strength and thermal stability ensure chip reliability under harsh conditions (Qi et al., 2018), whereas their favorable refractive index and infrared transparency facilitate the fabrication of photonic devices and enable precise optical detection (Kuzin et al., 2024). The fabrication of silicon-based microfluidic chips typically employs deep reactive ion etching (DRIE) or wet etching to create micro channels (Iyer et al., 2023). These processes can be integrated with chemical vapor deposition (CVD) and surface functionalization to improve biocompatibility (Batz et al., 2014; Liu et al., 2024; Juska et al., 2023). However, silicon-based chips face technical challenges, including high fabrication complexity (Qi et al., 2018; Kuzin et al., 2024), poor compatibility with optical microscopy (Skottvoll et al., 2024), and limited biocompatibility for long-term biological studies (Zhang et al., 2024).

Glass is widely employed in studies of multiphase flow within porous media due to its optical transparency, chemical stability, and high thermal resistance. These properties facilitate applications in diverse fields such as petroleum engineering (Gogoi et al., 2019), CO_2 sequestration (Hao et al., 2022; Li et al., 2024a), and multiphase reactive transport (Wei et al., 2024). Glass microfluidic chips are typically fabricated via wet etching or laser micromachining to create microchannels, which are then sealed through thermal bonding or adhesive bonding (Hwang et al., 2019). Moreover, their surface wettability can be precisely controlled via surface functionalization techniques (Silverio et al., 2019). Despite these advantages, the high cost and complex fabrication of glass microfluidic chips hinder their large-scale implementation. Future developments, including the integration of hybrid materials and optimized fabrication processes, are expected to improve their cost-effectiveness and broaden their applicability (Aralekallu et al., 2023).

PDMS is widely used to simulate multiphase flow in porous media (Lei et al., 2023a,b). Through soft lithography, PDMS enables the rapid fabrication of chips with intricate microchannels and pore structures (Rufai et al., 2018). This makes it suitable for replicating fluid dynamics in diverse porous media, including rocks and soil with varying porosity and permeability. However, PDMS has limited chemical resistance and degrades upon exposure to strong acids, bases, or organic solvents. This susceptibility restricts its use in high-temperature, corrosive environments (Battat et al., 2022), such as those involving oil displacement or supercritical CO_2-brine displacement processes. Tab. 1 summarizes the properties, advantages, and limitations of key materials used in fabricating microfluidic chips for multiphase flow studies.

3 Interfacial stability in two-phase flow

During CO_2 geological storage, both the injection phase and subsequent processes alter multiphase flow behavior in the reservoir. Interfacial instability can significantly impact storage efficiency (Bachu et al., 2015; Li et al., 2019; Yang et al., 2019). The displacement of brine by supercritical CO_2 typically occurs under low viscosity ratios, promoting unstable displacement and heterogeneous CO_2 flow pathways (Zhang et al., 2011). This heterogeneity causes uneven brine distribution within the pore space, influencing both the nucleation sites and morphology of salt precipitation (Shao et al., 2025). Localized water enrichment can create crystallization “hotspots”, where subsequent crystal formation modifies the pore structure and can lead to pore or throat blockage (Lönartz et al., 2023). Furthermore, pore-scale precipitation obstructs fluid flow and amplifies interfacial instability, reinforcing a detrimental feedback loop (Noiriel et al., 2016). As salt precipitation progresses and porosity evolves, flow dynamics and crystallization processes become increasingly coupled, generating complex feedback mechanisms (Ran et al., 2023; Li et al., 2024b).

The stability of the displacement process is governed by factors including porous media properties, fluid characteristics, and injection rate (Liu et al., 2016b; Lenormand et al., 1988). Controlled by the competition between capillary pressure and viscous forces, immiscible displacement in porous media may exhibit capillary fingering, viscous fingering, or a stable displacement front. Capillary fingering occurs when capillary forces dominate, whereas viscous fingering arises when viscous forces prevail (An et al., 2020). Characterizing flow patterns is essential for understanding the hydrodynamics of the displacement process. Researchers have established pore-scale phase diagram to classify displacement stability. Based on two dimensionless parameters - the viscosity ratio (M) and the capillary number (Ca) - the displacement regime is classified into three distinct types: viscous fingering (VF), capillary fingering (CF), and stable displacement (SD) (Zhang et al., 2011; Lenormand et al., 1988; Chen et al., 2023), see Fig. 3.

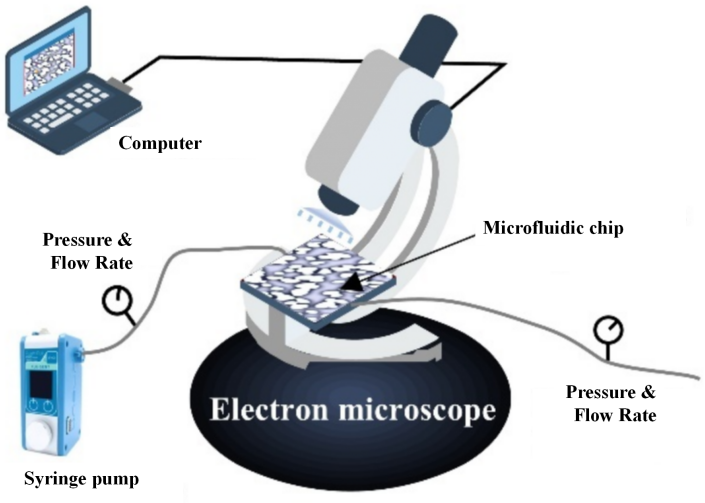

Fig. 2 Schematic of the micro visualization experimental setup

Tab. 1 Types of micro visualization chips

Materials	Advantages	Disadvantages	Topics
Silicon	Mechanical strength Thermal stability High refractive index Excellent optical electrical properties	Fragile High cost Difficult to process Incompatibility with optical microscopy	Biosensing (Liu et al., 2024; Juska et al., 2023) Neuroscience (Mu et al., 2023)
Glas, Quartz	High chemical resistance Optical transparency High pressure tolerance	Difficult to process Fragile High cost Hard to bond	Oil exploration (Gogoi et al., 2019) CO_2 sequestration (Hao et al., 2022) Multiphase reaction flow and mass transfer (Li et al., 2024b)
PDMS	Processing flexibility Transparency Low cost	Poor chemical resistance Poor heat resistance Easy to deformation	Suspension transportation and salt precipitation in porous media (Miri et al., 2015; Lei et al., 2023b)

3.1 Factors influencing interfacial stability

Studies indicate that increased wettability of the invading fluid toward the pore walls enhances interfacial stability during displacement (Jung et al., 2016; Holtzman et al., 2015). Avendaño et al. observed in core-flooding experiments that the water-oil interface is more stable in lipophilic media, indicating enhanced displacement stability when the invading fluid exhibits poor wettability to the pore walls (Avendaño et al., 2019). They attributed this behavior to the larger contact angle on hydrophobic surfaces, which reduces capillary pressure and thereby suppresses capillary instabilities like fingering. In core-flooding displacement experiments conducted by Wei et al (Wei et al., 2021), as the wettability between the invading phase and pore walls increased, capillary forces became more pronounced due to enhanced fluid-wall affinity. Consequently, the invading phase preferentially entered smaller pores while bypassing larger ones, trapping a significant portion of the displaced phase. Once trapped, the displaced phase resisted further mobilization, significantly reducing displacement efficiency. Additionally, capillary forces are influenced by flow rate (Hu et al., 2018). This apparent contradiction may arise from the competition between capillary and viscous forces. Zou et al. found that increasing flow rate reduced the influence of wettability on two-phase displacement patterns (Zou et al., 2020).

Pore-scale geometry significant influences interfacial dynamics. Wang et al. observed that increased particle angularity enhances surface-wettability heterogeneity within the fluid, consequently altering the macroscopic morphology of fluid invasion (Wang et al., 2021). Holtzman et al. proposed that heterogeneous pore-size distributions promote fluid-front tip splitting (Fig. 4a), which exacerbates fingering and reduces displacement efficiency (Holtzman et al., 2016). Subsequently, Rabbani et al. conducted displacement experiments using an ordered porous medium and found that a gradual increase in pore size along the flow path can suppress viscous fingering (Fig. 4b) (Rabbani et al., 2018). Furthermore, through numerical simulations, Suo et al. demonstrated that diverging pores (gradually increases size) stabilize the interface and enhance displacement efficiency, whereas converging pores (gradually decreases size) promote interfacial instability (Suo et al., 2024). However, the quantitative relationship between flow instability, pore geometry, and the underlying interfacial dynamics remains poorly understood.

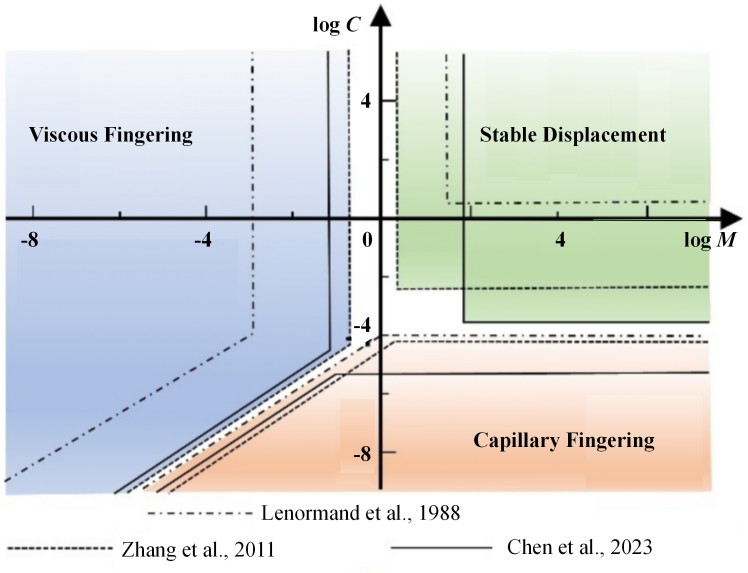

Fig. 3 Pore-scale displacement stability phase diagram

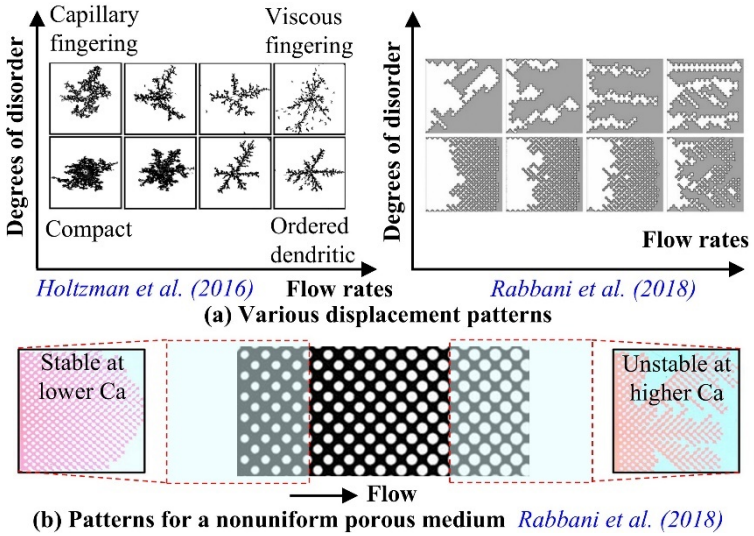

Fig. 4 Effects of pore size and internal topology on interfacial stability

3.2 Control of interfacial stability

Alterations in pore structure can affect local permeability, pore-throat distributions, and connectivity, thereby modifying capillary pressure gradients and flow resistance during interface propagation. Direct or indirect modifications of the pore structure are strategically employed to adjust fluid spatial distribution and flow pathways at the pore scale, thereby mitigating sudden breakthroughs or fingering phenomena. For example, Al-Housseiny et al. showed that varying the thickness of a Hele-Shaw cell (see Fig. 5) significantly suppresses viscous fingering during displacement, highlighting how pore-structure modifications control interfacial instability (Al-Housseiny et al., 2012).

Similarly, Wang et al. developed a controllable porous microfluidic device (PoroFluidics) (Wang et al., 2024b). Through precise regulation of solid geometry, wettability, and fluid properties, this device effectively suppresses interfacial instabilities in multiphase flows, enabling predictable and stable fluid invasion pathways. Furthermore, Lei et al. demonstrated that increasing the channel aspect ratio in microfluidic chips reduces imbibition-driven interfacial instabilities (Lei et al., 2023a).

Beyond geometric alterations, interfacial properties such as energy (e.g., surface tension) and wettability can be modulated by applying coatings with specific charges or functional groups to pore walls or particle surfaces (Kalde et al., 2022a). These coatings modify fluid-solid interactions by either promoting attachment or inducing repulsion, which subsequently alters the two-phase contact angle and displacement patterns. This approach to interfacial engineering provides a versatile strategy for controlling multiphase flow behavior. For example, Kalde et al. utilized polyelectrolyte coatings to manipulate the zeta potential of microfluidic channel surfaces (Kalde et al., 2022b). A negative surface potential, corresponding to poor wettability, promoted vigorous viscous fingering and resulted in low oil recovery. Conversely, a weakly positive potential markedly

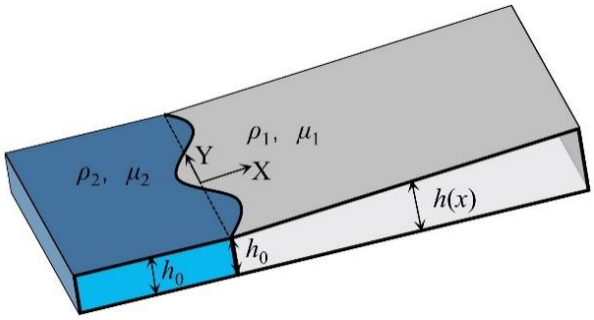

Fig. 5 Schematic diagram of a non-uniform Hele-Shaw cell with a constant depth gradient

suppressed interfacial instabilities and reduced fingering. A strongly positive potential yielded a stable interfacial morphology, demonstrating that increasing the positive surface charge effectively suppresses interfacial instabilities and improves displacement efficiency.

4 Investigating dry-out effects via microfluidic technology

Salt precipitation, induced by water evaporation during multiphase flow, is a key mechanism responsible for permeability impairment in high-salinity aquifers. Zuluaga and Monsalve investigated formation water evaporation during methane injection into both unconsolidated and consolidated sandstone cores, observing an absolute permeability reduction of approximately 14-30% (Zuluaga et al., 2003). Similarly, Peysson et al. injected nitrogen into consolidated sandstone cores (Peysson et al., 2014). Through pressure monitoring and X-ray imaging, they demonstrated that water evaporation triggers salt precipitation, which in turn significantly reduces core injectivity. Using micro-CT imaging in core-flooding experiments, Ott et al. observed that salt precipitation occurred predominantly near the injection inlet, coinciding with regions of residual water saturation (Ott et al., 2015). They attributed this phenomenon to solute enrichment from capillary-driven backflow, noting that such localized precipitation could enhance gas relative permeability (Fig.6). This conclusion, however, contrasts with the findings of Wang et al., who observed that CO_2 relative permeability was nearly halved (Wang et al., 2009). MRI images revealed that salt deposition clogged pore throats, thereby significantly impeding gas flow. These divergent results indicate that the impact of salt precipitation is highly dependent on specific conditions, a complexity that is difficult to resolve solely through core-flooding experiments.

The dry-out effect during displacement processes in porous media is governed by multiple factors, resulting in diverse salt precipitation patterns and varying impacts on reservoir properties. The specific manifestations of this process depend on the experimental conditions and core characteristics. This paper critically reviews recent advancements in studying the dry-out effect using microfluidic experiments.

4.1 Formation mechanism of salt precipitation

Salt precipitation morphology is primarily governed by liquid phase distribution and evaporation dynamics, and can be categorized into two distinct types: First, early-stage formation of bulk crystals within residual brine: These crystals nucleate at the solid-brine interface, growing into localized, massive structures. This process is driven by brine evaporation, which increases dissolved salt concentration until supersaturation and crystallization occurs. Second, the formation of aggregated polycrystalline structures at the gas-liquid interface, these widely distributed structures exhibit complex morphologies and are prevalent during advanced evaporation stages (Fig.7) (Miri et al., 2015; Zhang et al., 2024; Nooraiepour et al., 2018; Wu et al., 2023; Chen et al., 2024).

Ho and Tsai utilized a microfluidic platform to perform core-flooding experiments, elucidating the process of salt precipitation driven by drying in porous media (Ho et al., 2020). They classified this process into three distinct stages (Fig.7c): In the initial stage, salt crystals nucleate within isolated brine pockets (approximately one pore in size) and gradually develop into fine crystal clusters as drying progresses. In the rapid growth stage, abundant residual brine supplies ample solute, promoting the development of dendritic (feather-like) salt crystals that progressively occupy the pore space. In the final stage, capillary forces drive the migration of solute from the remaining brine, which deposits onto existing crystal surfaces, forming more complex aggregates. This characteristic Initial-rapid growth-final process was also observed in the experimental studies of Kim et al. and Miri et al (Kim et al., 2013; Miri et al., 2015). Similarly, Naillon et al. investigated salt crystals growth from supersaturated NaCl solutions in a microfluidic device (Naillon et al., 2017). They observed that during the initial phase, crystals grew rapidly due to the fast deposition of dissolved salts onto the crystal surface. Over time, however, the solute concentration near the crystal surface decreased, limiting ion transport and consequently slowing crystal growth. This growth inhibition occurs because crystal expansion gradually depletes salt content in the solution, while a diffusion boundary layer thickness further reduces the growth rate. Moreover, their results revealed that the observed precipitation rate substantially exceeded that predicted of classical diffusion-reaction theory.

Focusing on the polycrystalline aggregates, Miri et al. proposed a “self enhancement mechanism”, wherein a liquid film covering the salt surface transports brine to the evaporation front through the interconnected pore network of the hydrophilic matrix (Miri et al., 2015). This brine subsequently deposits onto the crystal surface, thereby promoting continued crystal growth. This process expands the available evaporation

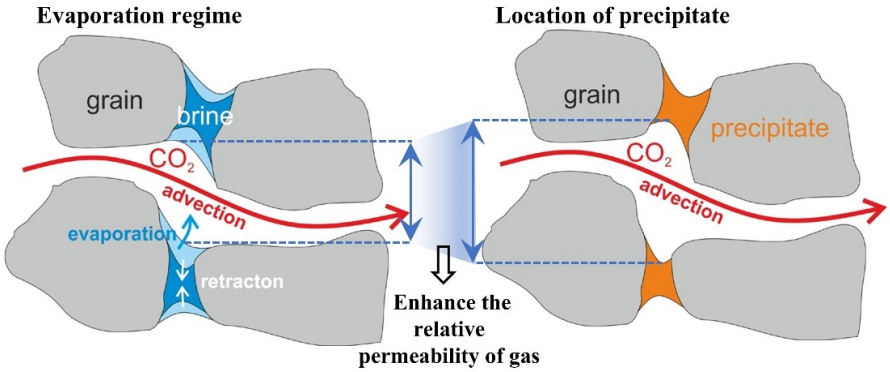

Fig. 6 Schematic of the dry-out and precipitation process

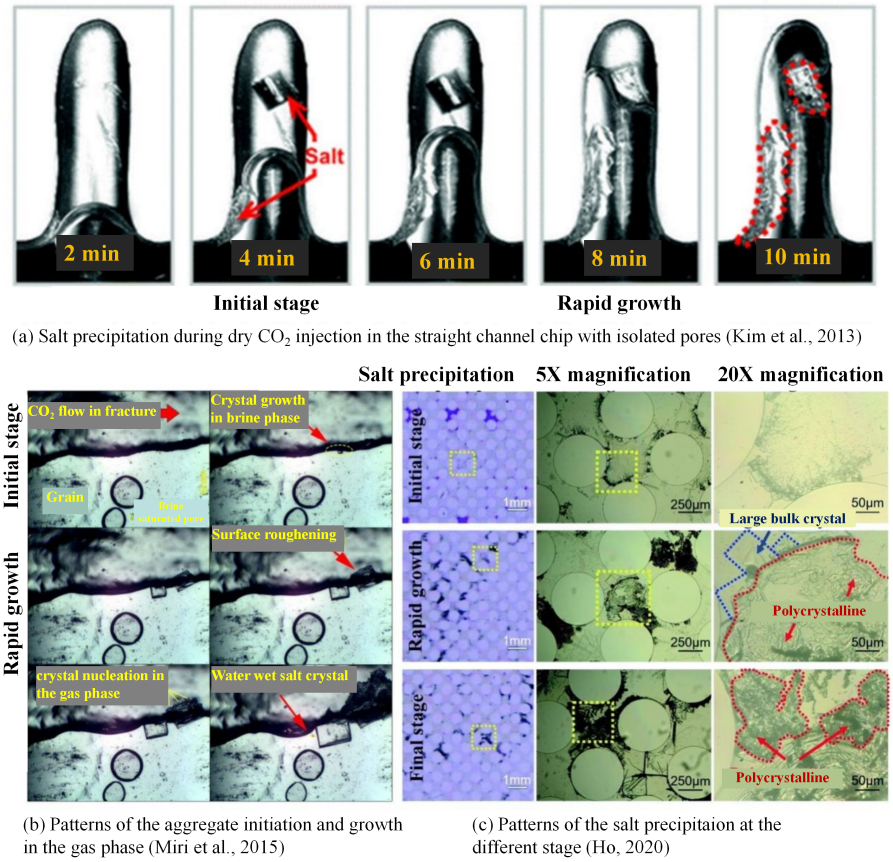

(a) Salt precipitation during dry CO_2 injection in the straight channel chip with isolated pores (Kim et al., 2013)

(b) Patterns of the aggregate initiation and growth in the gas phase (Miri et al., 2015)

(c) Patterns of the salt precipitaion at the different stage (Ho, 2020)

Fig. 7 Stages of drying and salt precipitation

area and markedly enhances the overall evaporation efficiency (Fig.8).

4.2 Influence of fluid properties on the drying effect

4.2.1 In situ aquifer salinity

According to Raoult's law, the solvent mole fraction in an ideal solution governs the evaporation process. As brine salinity increases, the equilibrium vapor pressure decreases, thereby reducing the evaporation rate (Guggenheim et al., 1937). Seo et al. observed a nonlinear relationship between evaporation rate and initial salinity: the rate initially decreases and then increases with rising salinity (Fig.9a) (Seo et al., 2019). This nonlinear trend is attributed to changes in the salt solution's activity coefficient. A decreasing activity coefficient enhances solvent-solute interactions, which inhibits water molecules escape and thus reduces the evaporation rate (Pitzer et al., 1984) (Fig.9b). Moreover, Rufai et al. demonstrated that increasing salt concentration significantly shortens the constant rate period (CRP) duration during evaporation (Rufai et al., 2017). Under saturated conditions (36% NaCl), the CRP nearly disappears (Fig.9c). During the CRP, the evaporation rate remains high and stable, resulting in a linear increase in mass loss over time.

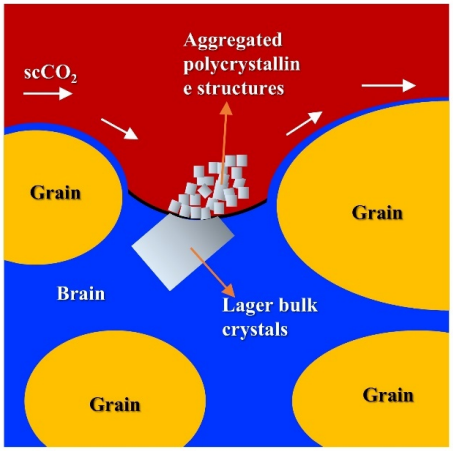

Fig. 8 Two types of salt crystals formed during displacement

However, at higher salinities, salt crystals gradually deposit on the porous medium surface, impairing capillary connectivity between the liquid phase and the evaporation front. Consequently, upon termination of CRP, the evaporation rate declines sharply, and mass loss becomes linearly proportional to the square root of time. This relationship indicates that evaporation is subsequently controlled by vapor diffusion and limited capillary flow.

Aquifer salinity is a key parameter controlling salt precipitation (Norouzi et al., 2021; Tang et al., 2015), as it directly determines the total dissolved salt content available for crystallization. Numerical simulations by Parvin et al. demonstrated that salinity governs both the onset and the extent of salt precipitation (Parvin et al., 2020). Specifically, higher salinity accelerates salt accumulation, leading to more severe permeability reduction.

Microfluidic studies corroborate that increasing solution salinity markedly enhances salt precipitation, thereby elevating the risk of crystallization-induced clogging and significantly reducing the porosity and permeability of porous media (Seo et al., 2019; Rufai et al., 2017; He et al., 2022). Some studies indicate that salt deposition and associated permeability impairment become negligible at salinities below 5 % (André et al., 2014). This view is supported by observations from the Sleipner field site in the North Sea, where a salinity of 3.5% and permeability of approximately 1 D have not resulted in reported impairment of injection capacity or well clogging to date. Wang et al. (2024) conducted displacement experiments using chips saturated with low-salinity solutions (10 % and 15 %) and high-salinity (20 % and 25 %) solutions, revealing distinct crystallization patterns. In low-salinity cases, crystals primarily formed as aggregated deposits within the extended channel and its single-pore branches. In contrast, high-salinity solutions generated large crystalline blocks. The main extended channel was often completely obstructed by sizable cubic crystals, with significant crystallization also occurring in the branch pores (Fig.10).

He et al. demonstrated that crystallization rates govern crystal morphologies; a low salinity, slower precipitation enables effective solution replenishment, promoting the development of aggregated crystals (He et al., 2023). In high-salinity brines, precipitation behavior can vary markedly even with minor salinity differences. For instance, Yan et al. reported that a minor salinity difference (e.g., 20% vs. 25%) can lead to distinct outcomes: 25% brine promotes rapid formation of large crystals, whereas 20% brine yields smaller, more dispersed crystals (Yan et al., 2025). Additionally, in 25% brine, multiple small grains can aggregate into branched or feather-like structures. These findings indicate that precipitation occurs not only as bulk deposits but also as polycrystalline aggregates at the gas-liquid interface, facilitated by liquid-film transport. This behavior may originate from uneven evaporation rates caused by gas-flow variations within the chip, combined with interactions between solute diffusion and liquid-film transport. For example, under high-salinity conditions (25%), rapid evaporation hinders timely replenishment at the evaporating front, resulting in larger crystals formation. Moreover, salinity variations alter wettability and modify the viscosity ratio between brine and CO_2 (Al-Khdheeawi et al., 2017), which promotes continuous brine replenishment and generates crystallization patterns distinct from those in high-salinity systems.

4.2.2 Injected fluid type

The viscosity ratio between the injected and resident fluids directly governs interfacial stability, consequently affecting residual water distribution and altering relative permeability (He et al., 2019b; Jeong et al., 2017). For commercial viability, potential CO_2 geological storage sites must maintain reservoir temperature and pressure conditions that keep CO_2 in a supercritical state (Chiquet et al., 2007). However, due to limitations in micro-scale visualization instrumentation, most experimental studies utilize gaseous CO_2 (Dąbrowski et al., 2025; Hu et al., 2022; Cheng et al., 2023). Although this approach cannot fully replicate the physical properties of supercritical CO_2, it still provides valuable insights into drying phenomena. Nooraiepour et al. conducted experiments involving simultaneous injections of gaseous, liquid, and supercritical CO_2 (Nooraiepour et al., 2018). Their results demonstrated that the CO_2 phase state substantially influence the extent and distribution of salt precipitation. Owing to its lower density and viscosity, gaseous CO_2 retains a higher residual water saturation during injection com-

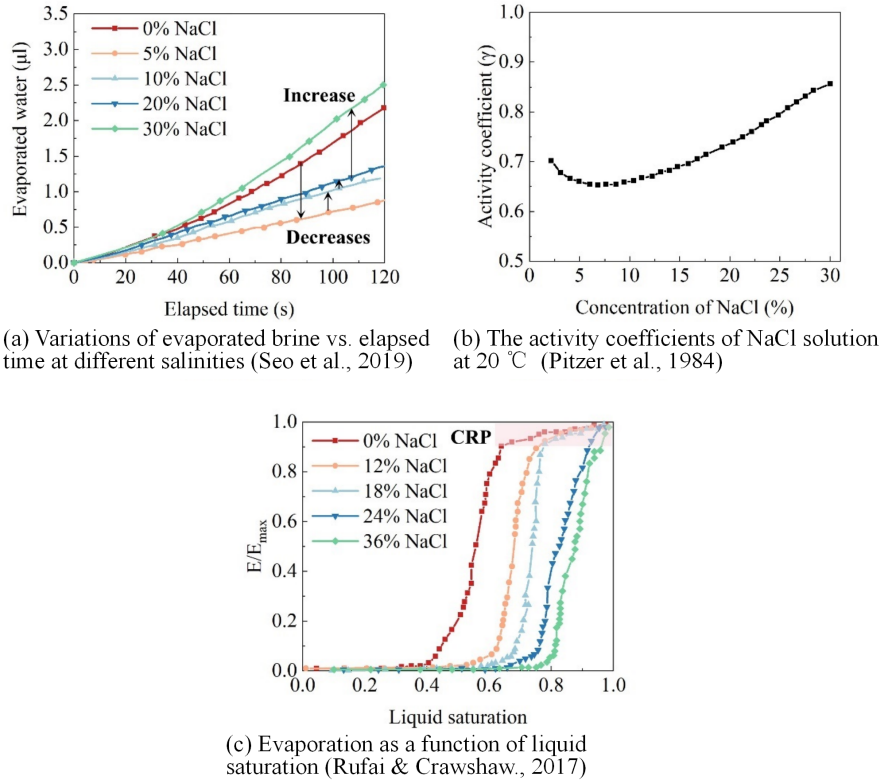

(a) Variations of evaporated brine vs. elapsed time at different salinities (Seo et al., 2019)

(b) The activity coefficients of NaCl solution at 20 ℃ (Pitzer et al., 1984)

(c) Evaporation as a function of liquid saturation (Rufai & Crawshaw., 2017)

Fig. 9 Effects of Salinity on Evaporation and Crystallization Rates

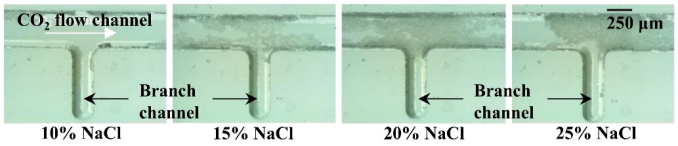

Fig. 10 Partial enlarged views of salt precipitation at different salinities

pared to liquid or supercritical CO_2. Consequently, the less efficient brine displacement enhances evaporation and solute concentration, ultimately resulting in extensive salt precipitation. Furthermore, to mitigate CO_2 instability and prevent corrosion from dissolved CO_2 in experimental apparatus, some core-scale and microfluidic-scale studies have employed N_2 (Lopez et al., 2020) or air (Chen et al., 2024) as substitutes for CO_2 in salt precipitation experiments. Chen et al. reported that salt crystals formed in air exhibit slightly lower hydrophilicity than formed those in CO_2, resulting in a marginally lower evaporation rate (Chen et al., 2024). Nonetheless, the overall salt precipitation processes in both environments are highly similar, suggesting that air-based experiments can yield valuable insights into precipitation behavior in CO_2 environments. However, due to the scarcity of comprehensive controlled experiments comparing different gases, the specific effects of gas types on the drying process remain incompletely understood.

4.3 Influence of flow conditions on the dry-out effect

4.3.1 Injection flow rate

The injection rate is a key control parameter during CO_2 injection. Several studies have investigated its influence on the dry-out effect using micro-scale visualization experiments (He et al., 2019b; Nooraiepour et al., 2018; He et al., 2022). An increased injection rate enhances brine displacement and suppresses capillary backflow (Jeddizahed et al., 2016); while simultaneously increasing the evaporation rate of residual brine. He et al. observed that at a low injection rate (0.1 mL/min), salt crystals predominantly deposited in the main channel, where CO_2 preferentially flows through path with larger pore throats and lower flow resistance (He et al., 2019b). At higher injection rates (0.5 and 2 mL/min), salt deposition in the main channel decreased significantly, but increased in adjacent regions with smaller pore throats. This distribution shift is attributed to capillary pressure variations across pore-throat structures. At lower rates, the gas displaces brine only near larger pore throats, concentrating the evaporation front and resulting in localized precipitation in the main channel. At higher rates, the increased injection pressure exceeds the capillary entry pressure of the smaller pore throats, enabling greater brine displacement and thereby reducing precipitation in the main channel.

4.3.2 Brine replenishment effect

He et al. and Wang et al. designed a microfluidic chip with

tree-shaped replenishment channels on both sides to simulate the brine replenishment mechanism within the boundary layer (Fig.11a) (He et al., 2024; Wang et al., 2023). Their experimental results demonstrated that continuous brine injection into these channels at a constant rate significantly increased the total salt precipitation. As shown in Fig.11b, salt precipitation was lower in the control group without brine supplementation. In contrast, the experimental group with brine supplementation, exhibited a significant increase in salt precipitation. Brine replenishment significantly influences both the formation process and spatial distribution of salt crystals. Under no-supplemented brine conditions, salt precipitation predominantly forms dispersed dendritic structures that are uniformly distributed throughout the pore space (Fig.11b). In contrast, under brine-supplemental conditions, especially at low CO_2 injection rates, salt crystals primarily accumulate near the inlet and form clustered ”wet salt” regions. At higher CO_2 injection rates, U-shaped salt bands form along the sides of the main flow channel and near the outlet.

Wang et al. emphasize that salt crystal growth is not unlimited, even with an adequate supply of supplemental brine (Wang et al., 2023). When the continuous brine influx is sufficient to flush the salt precipitation front, previously deposited salt dissolves, establishing a dynamic equilibrium between precipitation and dissolution. This equilibrium is evident in experiments with high brine supplementation rates (e.g., L-2 and H-2 groups) (Fig.11b), where porosity stabilizes and precipitation remains constrained despite an unrestricted brine supply. These findings demonstrate that an unlimited brine supply does not cause uncontrolled crystal growth. This conclusion was corroborated by core-flooding experiment in which Mascle et al. observed similar precipitation behavior (Mascle et al., 2023). They maintained capillary contact with supplemental brine to compensate for evaporation during gas injection.

4.4 Influence of pore medium characteristics on the dry-out effect

Rock porosity and permeability govern the overall capacity and efficiency of fluid storage and transport (Kang et al., 2019; Sibiryakov et al., 2021). Pore shape and size distribution influence salt crystal nucleation sites and growth rate (Nooraiepour et al., 2021). Small pore-throat radii or insufficient connectivity enable capillary forces to drive the preferential accumulation of salts within the pore space. Furthermore, variations in mineral composition and surface wettability alter salt deposition patterns and crystallization kinetics on pore surfaces (Dabrowski et al., 2024; Sun et al., 2024; Liefferink et al., 2018). Overall, porous medium characteristics govern both the formation and spatial distribution of salt crystals (Akindipe et al., 2021) and critically determine post-crystallization permeability and fluid transport efficiency.

4.4.1 Pore size

Low-permeability reservoirs are widely recognized to be more susceptible to permeability impairment from salt precipitation. The constricted pore structure in low-permeability reservoirs restricts fluid mobility, facilitating the localized accumulation of high-concentration brine and thereby promoting salt precipitation (Alizadeh et al., 2018). Existing studies on the dry-out effect often treat the pore network as a unified system, primarily emphasizing the impact of bulk reservoir properties on salt precipitation. However, they frequently overlook differential dry-out effects arising from pore-size variations at the individual pore scale. Capillary pressure differences arising from pore size heterogeneity cause solute to concentrate preferentially at pore throats or along pore walls (Lu et al., 2020). In smaller pores, stronger capillary forces enhance thin liquid films retention. In contrast, larger pores exhibit more rapid water loss due to weaker capillary forces, resulting in more pronounced drying. Consequently, pore-scale variations govern both the spatial-temporal patterns of salt nucleation and deposition and the distribution of capillary forces, ultimately determining flow dynamics and the degree of permeability impairment (Li et al., 2021; Yang et al., 2024).

To investigate pore-size effects on evaporation and salt precipitation distribution, Dong et al. conducted evaporation experiments using glass tubes with pore sizes of 1.0 mm, 1.9 mm, and 3.5 mm (Dong et al., 2024). Results demonstrated that smaller pores (1.0 mm) exhibited lower evaporation rates, attributed to stronger capillary forces and enhanced liquid transport that promoted salt accumulation at the meniscus. In contrast, the tube with the largest pore size (3.5 mm) exhibited the highest evaporation rate, with rapid liquid-front retreat resulting in a more dispersed salt distribution (Fig.12). Although the millimeter-scale circular capillaries in this experiment are significantly larger than the micrometer-sized to nanometer-sized pores in deep saline aquifers, and the evaporation behavior relied on single-channel liquid-front advancement (unlike the complex multiphase behavior in porous media), this study provides valuable mechanistic insights. It reinforces that pore size influences both salt crystals distribution and the drying process, suggesting that findings from idealized geometries can inform salt solution evaporation in complex porous media.

4.4.2 Pore heterogeneity

Microfluidic visualization chips, fabricated from actual rock samples or vis artificial design, serve as excellent tools for investigating heterogeneity in porous media. Whole-process visualization of the dry-out effect reveals that in heterogeneous pore structures, gas preferentially flows through larger pores, establishing dominant flow paths. Consequently, heterogeneous structures exhibit significantly lower displacement efficiency than homogeneous ones (Qian et al., 2025). Furthermore, salt precipitation typically follows a multi-stage process that spans from initial dissolution and evaporation to final precipitation, with each stage being influenced by heterogeneous factors such as pore size, connectivity, and fracture distribution. This influence manifests as spatial variations in crystal size and crystallization rate across different regions (Dashtian et al., 2018).

He et al. designed three types of heterogeneous microfluidic chips with distinct structural configurations, namely up-down heterogeneous, left-right heterogeneous, and a composite structure containing fractures (Fig.13a), to investigate the drying effect (He et al., 2023). Their study revealed that in heterogeneous structures, low injection rates mitigate precipitation-induced clogging by modifying flow pathways and redistribut-

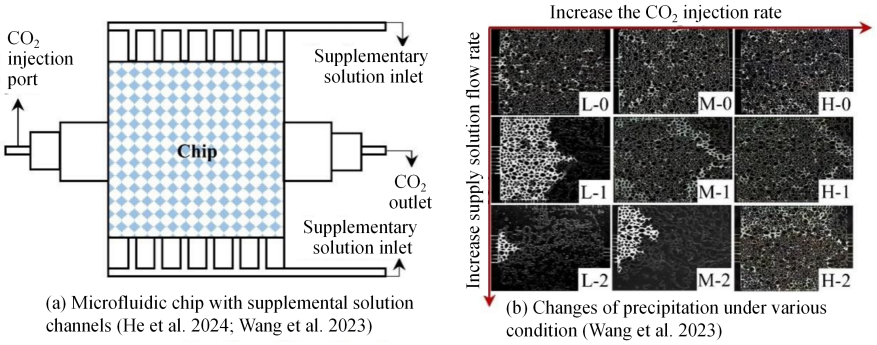

Fig. 11 Brine replenishment mechanism within the boundary layer

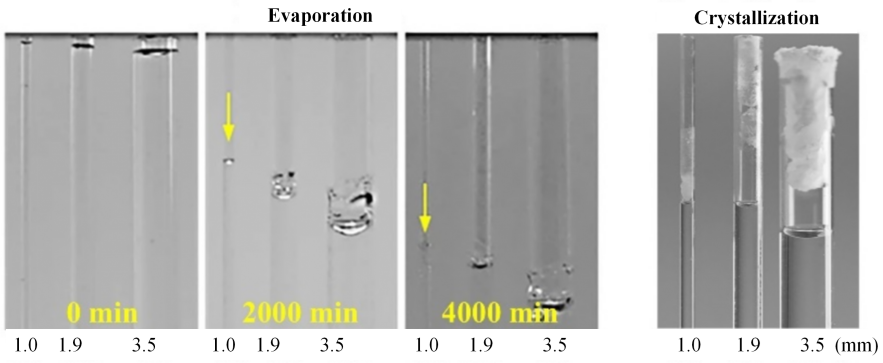

Fig. 12 Evaporation Experiments in Capillary Glass Tubes with Different Pore Sizes

ing residual brine. This flow redistribution disperses salt deposition into small-pore regions, preventing excessive accumulation at the inlet and in primary flow channels. Furthermore, low injection rates reduce the evaporation rate, allowing the brine to redistribute via diffusion, which further inhibits localized salt concentration. In the composite structure, salt deposition within fractures can induce a ”self-healing” effect that helps maintain open flow pathways.

Nooraiepour et al. similarly highlighted that widely distributed salt crystals within fractures can act as a “healing” mechanism, which under certain conditions may reduce the risk of CO_2 leakage (Nooraiepour et al., 2018). Building on this concept, heterogeneity can mitigate clogging by optimizing the spatial distribution of salt precipitation, offering a novel perspective on reservoir design (He et al., 2023). However, large-scale numerical simulations have demonstrated that heterogeneity reduces wellbore injectivity (Rasmusson et al., 2016; Nordbotten et al., 2005; Al-Khdheeawi et al., 2018). Ren et al. further argued that simplifying highly heterogeneous reservoirs into a deterministic multiphase model could significantly underestimate the drying effect (Ren et al., 2021). Moreover, the layered structures used in experimental studies primarily simulate simplified upper-lower or left-right pore distributions. Whether such simplified model can adequately capture the complex, stochastic heterogeneity of most reservoirs remains an open question requiring further validation.

Zhang et al. employed pore networks with randomly distributed pore sizes (Chips 1-3), where heterogeneity increased progressively from low to high (Fig.13b) (Zhang et al., 2024). Their results indicated that as heterogeneity increased, permeability reduction from salt precipitation rose from 65 % to approximately 80 %, demonstrating that heterogeneous structures are more susceptible to localized plugging. Additionally, dominant flow paths in highly heterogeneous chips l promoted residual brine retention in specific regions, sustaining local salt enrichment and further exacerbating permeability reduction. Yan et al. observed that regions with poor connectivity exhibited more dispersed and irregular salt crystal distributions (Fig.13c) (Yan et al., 2025). Residual brine distribution was significantly influenced by pore structure heterogeneity. More homogeneous structures resulted in less brine accumulation near the injection port, thereby reducing salt precipitation in this region. Furthermore, Yan et al. conducted displacement experiments in both flow directions on the same chip, finding that injection direction had little impact on overall salt precipitation distribution in homogeneous media (Yan et al., 2025). However, in heterogeneous media, the salt precipitation pattern was notably altered by pore structure anisotropy.

The studies by He et al. and Zhang et al. both confirmed the critical regulatory role of heterogeneity in drying and salt precipitation processes (He et al., 2023; Zhang et al., 2024). However, notable differences exist between these studies in their construction of heterogeneous structures and the manifestation of salt precipitation. The former emphasizes how heterogeneity mitigates clogging and promotes self-healing mechanisms, whereas the latter focus on salt retention in randomly distributed pore spaces and the resulting permeability impairment. Combined with Yan et al. analysis of injection direction effects (Yan

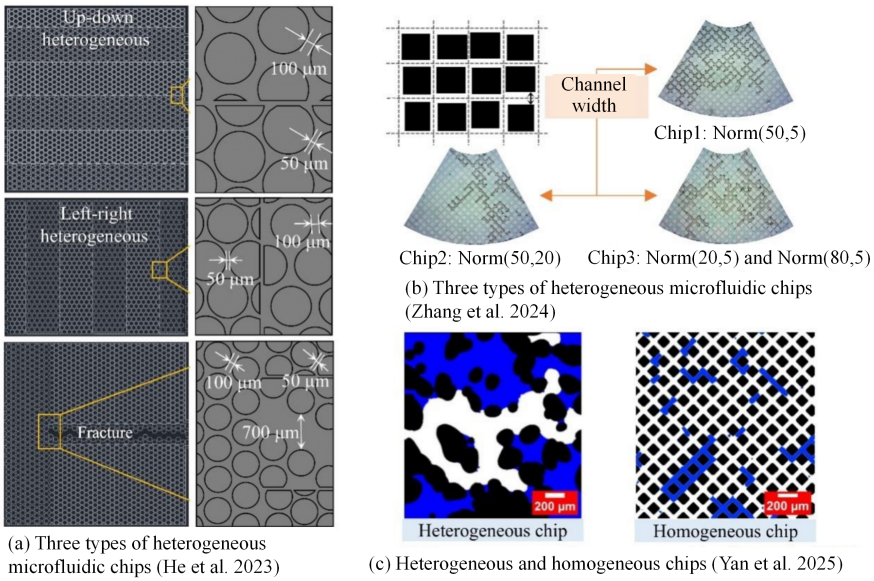

(a) Three types of heterogeneous microfluidic chips (He et al. 2023)

(b) Three types of heterogeneous microfluidic chips (Zhang et al. 2024)

(c) Heterogeneous and homogeneous chips (Yan et al. 2025)

Fig. 13 Diagram of different heterogeneous micromodel structures

et al., 2025), it is evident that heterogeneity and its anisotropy govern not only the spatial distribution of salt precipitation but also the drying pattern and the extent of permeability impairment.

4.4.3 Wettability

Rock wettability plays a critical role in interfacial stability by regulating fluid migration and distribution, thereby influencing the formation and spatial distribution of salt crystals. Microfluidic techniques enable the fabrication of chips with tunable wettability via various surface modification methods, such as plasma treatment (Li et al., 2024b), UV-induced graft polymerization (Schneider et al., 2010), chemical vapor deposition (CVD) of trimethoxy silane (Zhao et al., 2016), surface chemical coating (Hossain et al., 2024), laser etching (Wang et al., 2011), and electrowetting (Kalde et al., 2022b). These techniques allow researchers to precisely manipulate surface wettability to explore wettability-driven interfacial phenomena in porous media.

Experimental studies on the dry-out effect in chips with varying wettability reveal significant differences in drying modes, salt morphology, and precipitation distribution between hydrophobic and hydrophilic systems. Wettability directly influences the drying process and residual brine distribution. Zhang et al. demonstrated that in hydrophilic pores, a continuous liquid film facilitates capillary reflux (Zhang et al., 2024). This accelerates the drying process and concentrates brine at the evaporation front. Consequently, salt precipitation becomes more concentrated and crystallization denser. Similarly, Dabrowski et al. observed that in hydrophilic environments, enhanced liquid film flow promotes more active precipitation and the development of larger, irregular crystal structures (Dąbrowski et al., 2025). In contrast, in hydrophobic media, drying is slower due to liquid film rupture and limited capillary reflux, resulting in more discrete precipitation and smaller, dispersed crystals. Furthermore, wettability governs the spatial distribution and morphology of salt precipitation. He et al. emphasized that in hydrophilic media, precipitation tends to occur outside the pore channels (ex-situ), causing more severe pore plugging and permeability reduction (He et al., 2019b). In contrast, in hydrophobic environments, precipitation is more likely to occur within the pore space (in-situ), resulting in deposition and a reduced impact on permeability. Yan et al. further found that hydrophilic pores in highly heterogeneous regions exhibit more irregular and spatially variable precipitation distributions (Yan et al., 2025). Some areas formed large crystal aggregates, whereas others showed minimal deposition. Although these studies vary in experimental design and specific precipitation patterns, they concur on a key point: In hydrophilic networks, enhanced capillary reflux and persistent liquid film flow accelerate drying, leading to higher brine concentration, more severe precipitation, and significant permeability impairment. In contrast, hydrophobic media inhibit liquid film flow, resulting in more dispersed precipitation and a reduced overall impact on permeability.

Rock-fluid interactions and changes in reservoir fluid conditions can alter rock wettability (Maes and Geiger, 2018). CO_2 injection induces the release and adsorption of organic acids (e.g., lignoceric acid), leading to wettability modifications. Even at low concentrations, organic acids can form chemisorbed layers on rock surface, gradually transforming initially hydrophilic formations into neutral or hydrophobic ones (Ali et al., 2020). Natural reservoir rocks often exhibit mixed wettability, characterized by a non-uniform distribution that forms localized hydrophilic and hydrophobic domains. This heterogeneity can result in continuous hydrophobic or hydrophilic channels, or alternating wettability along a single flow path (Civan, 2023). Recent studies have investigated multiphase flow behavior and front propagation under mixed-wettability conditions (Da Wang et al., 2024; Sun et al., 2024; Akai et al., 2019; Scanziani et al., 2020; Gao et al., 2020). These studies have provided insights into the effects of mixed wettability on fluid percolation (Irannezhad et al., 2023), bound water

saturation (Kim et al., 2025), and capillary pressure profiles (Hiller et al., 2019). AlOmier et al.employed a lithography-assisted, selectively patterned silanization technique to generate controlled mixed-wettability conditions in a microfluidic device. In their approach, pore-throat regions intended to remain hydrophilic were protected using a photolithographic mask, followed by fluorosilane (FDTS) vapor deposition onto the exposed surfaces. Removal of the photoresist preserved the native hydrophilicity of the masked areas while rendering the exposed regions hydrophobic, thereby creating a spatially defined wettability contrast within the pore network. Using this mixed-wet microfluidic platform, the authors demonstrated that fluid flow under heterogeneous wettability is not simply an intermediate case between uniformly hydrophilic and uniformly hydrophobic systems; rather, distinct displacement behaviors emerge, governed by the distribution and balance of hydrophilic and hydrophobic regions (AlOmier et al., 2024). In fully hydrophobic chips, high injection pressures result in low displacement efficiency and significant gas retention. In fully hydrophilic chips, injection pressures are lower and flow through larger pore channels is significant, but some regions remain upswept. In Mix-Med and Mix-High systems (with a higher proportion of hydrophilic regions), breakthrough times and pressures are significantly reduced. The fluid front is more continuous and displacement efficiency is higher, outperforming fully hydrophobic chips and approaching the efficiency of fully hydrophilic systems. However, in Mix-Low systems (with low proportion of hydrophilic regions), the sparse distribution of hydrophilic domains limits flow paths, reducing displacement efficiency. Nevertheless, research on the drying effect following CO_2 injection under mixed wettability conditions remains scarce. Most existing studies focus on uniform wettability conditions (He et al., 2019b; Zhang et al., 2024; Yan et al., 2025) and do not fully address local crystallization differences and drying processes resulting from uneven wettability distribution on pore surface. Understanding these localized drying effects is essential for accurately predicting salt precipitation behavior and its impact on reservoir permeability after CO_2 injection.

4.4.4 Injection strategies for mitigating salt precipitation

Salt precipitation can be mitigated through various strategies, including pre-injection of freshwater or low-salinity brine, selecting high-quality reservoirs, employing high injection rates, implementing alternating gas-liquid injection, and applying acid treatments (Smith et al., 2022; Zhang et al., 2025; Rathnaweera et al., 2016; Darkwah-Owusu et al., 2024). Among these, alternating gas-liquid injection is a widely employed engineering strategy. Moreover, fluctuations in injection rates and intermittent well shut-ins, which are inevitable during actual CO_2 storage operations, can be considered a passive form of gas-liquid alternating injection. Seo et al. demonstrated through microfluidic experiments that sequential water-CO_2 injection effectively mitigates the drying effect (Seo et al., 2019). Their results revealed that sequential injection significantly reduced salt precipitation and produced a more dispersed crystal distribution. In contrast, conventional CO_2 injection resulted in more concentrated deposition at the evaporation front. This strategy not only mitigated the drying effect and reduced salt deposition but also enhanced the gas-liquid interfacial area by generating micro-CO_2 bubbles. This facilitated CO_2 dissolution in brine and improved sequestration efficiency (Li et al., 2023). Furthermore, measurements of residual water saturation and evaporation rates under this strategy showed that brine evaporation rates were reduced to one-fifteenth of those under conventional dry CO_2 injection. Additionally, He et al. proposed a variable-rate injection strategy that avoided excessive brine reflux at the inlet by switching from a low to a high CO_2 injection rate (He et al., 2024). This strategy helped reduce localized salt aggregation.

5 Discussion

5.1 Advantages of microfluidic visualization techniques

Common visualization techniques for studying multiphase flow include CT scanning, MRI, and others. Compared to these traditional methods, microfluidic visualization techniques offer distinct advantages. Mascini et al. employed CT scanning to investigate multiphase flow in porous media, providing three-dimensional (3D) fluid distribution and structural information within pore spaces (Mascini et al., 2021). However, the limited spatial resolution of CT imaging challenges the capture micro-scale fluid dynamics. Additionally, CT imaging suffers from insufficient temporal resolution, a single scan can take several minutes (Zwanenburg et al., 2021), preventing real-time observation of rapid capillary instabilities. This limitation hinders precise characterization of fluid-front evolution and interfacial dynamics. In their study of the dry-out effect, Akindipe et al were constrained by time resolution, necessitating a reduction in the injection rate to an extremely low value (0.0005 cm^3/min) prior to each image acquisition (Akindipe et al., 2022). This approach minimized fluid movement during scanning, enabling more stable imaging but compromising the observation of real-time flow dynamics. Similarly, MRI faces challenges in capturing fast transient multiphase flows, particularly in high-velocity regimes or environments with short relaxation times, making accurate tracking of fluid-front migration difficult (Elsayed et al., 2022). These limitations restrict the ability of these techniques to capture realistic transient flow processes.

In contrast, microfluidic visualization enables real-time, high-frame-rate recording of experimental processes, with resolution depending on the camera system. Sun et al. utilized microfluidic visualization to investigate fluid flow through porous media (e.g., Haines jump), successfully capturing invasion, interfacial motion and phase distribution at the microscopic scale (Sun and Santamarina, 2019). Owing to its high spatial and temporal resolution, microfluidic visualization is well-suited for studying salt precipitation and interfacial dynamics, providing the precision necessary to resolve pore-scale fluid interactions and interfacial behavior. A key advantage of microfluidic systems is their customizable chip designs, which can be tailored to replicate specific pore structures or flow pathways for diverse research applications. For example, Wang et al. fabricated a synthetic $CaCO_3$ reservoir micromodel whose surface was entirely covered with calcite, enabling investigations of mineral-fluid interactions (Wang et al., 2017). Wei et al. developed a

multicomponent porous structure within a glass microchannel, enabling pore-scale visualization of calcite dissolution (Wei et al., 2024). Massimiani et al. employed image-based etching techniques, utilizing 3D thin-section images of Houston rocks to fabricate realistic core-etched microfluidic chips (Massimiani et al., 2023). This approach bridges the gap between study of synthetic and natural porous media.

Compared to traditional imaging techniques such as CT and MRI, microfluidic visualization systems provide a cost-effective alternative, typically requiring only a camera, a syringe pump, and a microfluidic chip (Wu et al., 2024; Lake et al., 2017; Jahanbakhsh et al., 2020). Furthermore, microfluidic setups are compact, easily designed, and straightforward to operate. They enable precise regulation of fluid flow and pressure using simple equipment (e.g., syringe pumps), eliminating the need for complex sample preparation or large-scale imaging systems.

Overall, despite limitations in replicating fully 3D structures, adapting to extreme environmental conditions, and extrapolating macroscopic data, operational simplicity, microfluidic visualization systems remain an indispensable tool for investigating complex multiphase flow dynamics due to their low cost, operational simplicity, and rapid feedback capabilities.

5.2 Challenges in microfluidic experimental methods for studying dry-out phenomena

Most current microfluidic studies of salt precipitation are confined to single-depth, two-dimensional (2D) chips. In 2D chips, the pore structure is compressed into a planar configuration. This geometry restricts fluid flow pathways, interfacial contact between the brine and solid phase, and crystal nucleation and growth to a single plane. This simplified geometry fails to capture the complex connectivity and gravitational effects characteristic of real reservoirs, where fluid migration and salt deposition occur within a multi-scale, vertically interconnected pore-throat network. Furthermore, visualizing the dynamic evolution of pore structures, which is driven by stratigraphic stress or localized fluid-solid interactions, remains challenging in planar systems and leads to discrepancies between experimental observations and actual reservoir conditions. Consequently, accurately replicating the intricate 3D processes governing salt precipitation in natural porous networks remains a significant challenge. Advancements in microfluidic technology are addressing these limitations. Lei et al. developed chips with varied depth layouts, effectively overcoming the constraints of traditional 2D chips, which inadequately simulate the diverse pore-size distributions of natural 3D porous media. These advanced chips have demonstrated significant advantages for studying multiphase displacement and interfacial stability (Lei et al., 2024). Moreover, zeta potential measurements are well-established in core-flooding experiments for evaluating how brine composition affects surface potential and local wettability (Abbasi et al., 2022). However, this approach has not been fully integrated into microfluidic investigations of salt precipitation. Combining multi-depth chips with zeta potential modulation to examine crystallization kinetics during displacement could provide comprehensive insights into precipitation mechanisms and yield new strategies for controlling precipitation in engineering applications, whether by inhibiting or promoting deposition in specific regions.

Microfluidic technology enables the systematic investigation of factors influencing salt precipitation by controlling boundary conditions, such as brine availability (Wang et al., 2024a), injection rate (He et al., 2024), and salinity (Yan et al., 2025). Although significant progress has been made in understanding the driving mechanisms, interfacial stability, and key factors of salt precipitation, most experiments are conducted under idealized conditions. In these studies, temperature, pressure, and fluid composition are tightly controlled, and chip designs are simplified (homogeneous/heterogeneous patterns or rock slices) (Li et al., 2024c). In contrast, natural subsurface formations exhibit far greater complexity. The presence of heterogeneous or fractured 3D rock networks (Zhou et al., 2022), multiphase fluid interactions (Cai et al., 2024), and depth-dependent variables such as temperature, pressure gradients, and geomechanical stresses (Bohnsack et al., 2021) significantly complicates the salt precipitation process and makes it challenging to replicate under laboratory conditions.

Microfluidic visualization is a valuable tool for investigating salt precipitation processes. However, quantifying the kinetic of nucleation and growth at the pore scale remains challenging, and real-time observation of salt precipitation across specific regions of complex porous media networks has not been achieved. Furthermore, the prolonged evaporation times required for salt precipitation necessitate continuous manual monitoring, further complicating experimental procedures. Nonuniform evaporation rates, induced by variations in pore-scale gas flow velocity, govern the formation and evolution of different precipitation morphologies (e.g., polycrystalline clusters and bulk crystals) through their control on solute diffusion rates and liquid-film transport mechanisms. However, a comprehensive mechanistic understanding of these interactions remains lacking. Furthermore, different crystallization patterns affect permeability differently, potentially leading to biased assessments of precipitation risks and pore evolution in reservoirs (Jannesarahmadi et al., 2024). This complexity challenges the accurate integration of multiple coupling effects into predictive models, thereby compromising the reliability of forecasts for the safety and efficacy of geological storage.

5.3 Discussion of future development

The relationship between salinity and salt precipitation is not purely linear but results from complex interactions among multiple factors. High salinity enhances salt precipitation while impeding fluid movement and altering overall evaporation dynamics. Future research should focus on unraveling these interdependent mechanisms through multi-factor coupled experimental designs to quantitatively assess salt crystal growth kinetics under diverse conditions. Integrating multi-depth microfluidic chips with X-ray and CT imaging will enable 3D visualization of salt precipitation, offering deeper insights into the interplay between evaporation dynamics and fluid transport. Experimentally derived precipitation kinetics can be incorporated into multiphase flow models, facilitating the transition of pore-scale

observations to field-scale predictions. These advancements will significantly improve the understanding of precipitation behavior in geological sequestration environments.

Studies on crystallization within nanoscale pores in materials science have provided valuable mechanistic insights (Roosta et al., 2024; Scherer, 1999). For example, Galloway et al. demonstrated that calcium sulfate crystallization within 200 nm, 25–100 nm, and 10 nm pores formed oriented gypsum, bassanite, and anhydrite, respectively (Galloway et al., 2023). Nanoscale pores confinement influence crystallization dynamics, including nucleation rate, crystal phase, size, morphology, and orientation (Xing et al., 2022). However, comprehensive experimental and numerical evidence remains limited for micron-scale pores, which dominate geological sequestration environments. Future research on pore-scale variations in dry-out effect is crucial to improve the understanding of salt precipitation mechanisms in CO_2 geological storage and to establish a more robust scientific framework for reservoir safety assessment and management.

Achieving precise control over injection sequences and flow rate remains a significant technical challenge in mitigating salt precipitation through alternating gas-liquid injection. Rapid fluid switching may induce local flow instabilities, which can compromise experimental accuracy and reproducibility. Additionally, acidic water formed by CO_2 dissolution can dissolve reservoir minerals, increasing porosity. This poses a challenge for adjusting experimental materials to accurately replicate these dissolution effects during fluid displacement. Furthermore, brine replenishment can dissolve previously deposited salt, leading to a dynamic equilibrium between precipitation and dissolution. Understanding how this equilibrium influences porous media injectivity has significant engineering implications, particularly since alternating gas-liquid injection is an unavoidable aspect of actual CO_2 injection processes.

Analysis of formation water crystallization dynamics indicates that precipitated salt particles can undergo settling, capture, or bridge plugging within pore throats, representing key transport behavior of crystalline solid. At low flow velocities, salt particles settle under gravity, whereas at higher velocities, they may be captured in pore throats or form bridge plugs (Wang, 2016). However, these phenomena have not been directly observed in microfluidic experiments, likely due to two key factors: 1) Scale limitations: Microfluidic systems operate at small scales with low fluid velocities and shear forces, which are often insufficient to induce significant particle transport. 2) Neglect of gravity: Most microfluidic experiments neglect gravitational effects, making it difficult to observe particle settling under low-flow conditions. These limitations highlight significant discrepancies between microfluidic experimental conditions and natural crystallization environments. Therefore, optimizing experimental designs to better replicate natural environments and enable the observation of particle settling, capture, and bridge-plugging behaviors remains a major research challenge.

6 Conclusion

This review systematically examines the application of micro visualization techniques for studying the dry-out effect in porous media, summarizing current research progress and key findings. It provides an in-depth analysis of the formation mechanisms and key factors governing interfacial stability and dry-out effects, emphasizing the coupled interactions among fluid properties, flow conditions, and pore structure characteristics during displacement and salt precipitation processes. This review aims to provide insights and references for future studies on salt precipitation mechanisms and the optimization of geological storage strategies. It also offers valuable perspectives for salt precipitation research in porous media across various scientific and engineering disciplines.

The key conclusions are as follows:

a. Micro visualization experiments enable real-time monitoring of pore-scale fluid dynamics, offering superior temporal and spatial resolution over traditional imaging techniques like CT and MRI. These techniques enable direct observation of gas-liquid interface evolution and salt crystal growth, providing an indispensable platform for investigating interactions between pore structure, wettability, and salt precipitation.

b. Salt precipitation is primarily induced by water evaporation during displacement and is strongly influenced by pore geometry, flow rate, and wettability. High salinity environments exacerbate the risk of salt precipitation-induced plugging. Furthermore, variations in injection rates, gas-liquid alternating strategies, and brine replenishment patterns critically govern the distribution and extent of salt precipitation, thereby differentially affecting permeability and injectivity.

c. In heterogeneous and mixed-wettability porous media, pore structure governs the distribution of preferential flow paths and residual water, whereas wettability influences fluid transport through liquid films. These coupled effects promote localized salt crystal accumulation, which can cause pore plugging and contribute to fracture self-healing. The spatial distribution of wettability regions and pore size variations influence both evaporation dynamics and crystal morphology, highlighting the need for more targeted engineering control strategies.

d. Dynamic visualization of salt precipitation under in-situ conditions remains limited, and the integration of pore-scale observations into multi-scale modeling frameworks is still insufficient. Future work should therefore strengthen in-situ visualization capabilities to better resolve mass-transfer processes, liquid-film transport and the dynamic evolution of pore structures during salt precipitation. In parallel, improving multi-scale modeling integration is essential for linking pore-scale mechanisms to reservoir-scale predictions, thereby enhancing the assessment of CO_2 injectivity, storage safety and long-term performance.

Acknowledgements

The authors are grateful for the support from the National Natural Science Foundation of China (Grant No. 52209129, U23B20144).

Conflict of interest

The authors declare no competing interest.

References

Abbasi P, Madani M, Abbasi S, et al. 2022. Mixed salt precipitation and water evaporation during smart water alternative CO_2 injection in carbonate reservoirs. *Journal of Petroleum Science and Engineering*, **208**: 109258. doi:10.1016/j.petrol.2021.109258.

Akindipe D, Saraji S, Piri M. 2021. Salt precipitation during geological sequestration of supercritical CO_2 in saline aquifers: A pore - scale experimental investigation. *Advances in Water Resources*, **155**: 104011. doi:10.1016/j.advwatres.2021.104011.

Akindipe D, Saraji S, Piri M. 2022. Salt precipitation in carbonates during supercritical CO_2 injection: A pore-scale experimental investigation of the effects of wettability and heterogeneity. *International Journal of Greenhouse Gas Control*, **121**: 103790. doi:10.1016/j.ijggc.2022.103790.

Akai T, Alhammadi AM, Blunt MJ, et al. 2019. Modeling oil recovery in mixed-wet rocks: pore-scale comparison between experiment and simulation. *Transport in Porous Media*, **127**: 393–414. doi:10.1007/s11242-018-1198-8.

Al-Housseiny TT, Tsai PA, Stone HA. 2012. Control of interfacial instabilities using flow geometry. *Nature Physics*, **8**(10): 747 - 750. doi:10.1038/nphys2396.

Al-Khdheeawi EA, Vialle S, Barifcani A, et al. 2017. Effect of brine salinity on CO_2 plume migration and trapping capacity in deep saline aquifers. *The APPEA Journal*, **57**(1): 100 - 109. doi:10.1071/AJ16248.

Al-Khdheeawi EA, Vialle S, Barifcani A, et al. 2018. Effect of wettability heterogeneity and reservoir temperature on CO_2 storage efficiency in deep saline aquifers. *International Journal of Greenhouse Gas Control*, **68**: 216 - 229. doi:10.1016/j.ijggc.2017.11.016.

Alizadeh AH, Akbarabadi M, Barsotti E, et al. 2018. Salt precipitation in ultratight porous media and its impact on pore connectivity and hydraulic conductivity. *Water Resources Research*, **54**(4): 2768 - 2780. doi:10.1002/2017WR021194.

Ali M, Aftab A, Arain ZUA, et al. 2020. Influence of organic acid concentration on wettability alteration of cap-rock: implications for CO_2 trapping/storage. *ACS Applied Materials & Interfaces*, **12**(35): 39850–39858. doi:10.1021/acsami.0c10491.

AlOmier A, Hoecherl M, Cha D, et al. 2024. Experimental Investigation of the Impact of Mixed Wettability on Pore-Scale Fluid Displacement: A Microfluidic Study. *ACS Applied Materials & Interfaces*, **16**(50):69165–69179. doi:10.1021/acsami.4c13018.

An S, Erfani H, Godinez - Brizuela OE, et al. 2020. Transition from viscous fingering to capillary fingering: Application of GPU - based fully implicit dynamic pore network modeling. *Water Resources Research*, **56**(12): e2020WR028149. doi:10.1029/2020WR028149.

André L, Peysson Y, Azaroual M. 2014. Well injectivity during CO_2 storage operations in deep saline aquifers–Part 2: Numerical simulations of drying, salt deposit mechanisms and role of capillary forces. *International Journal of Greenhouse Gas Control*, **22**: 301 - 312. doi:10.1016/j.ijggc.2013.10.030.

Aralekallu S, Boddula R, Singh V. 2023. Development of glass-based microfluidic devices: A review on its fabrication and biologic applications. *Materials & Design*, **225**: 111517. doi:10.1016/j.matdes.2022.111517.

Avendaño J, Lima N, Quevedo A, et al. 2019. Effect of surface wettability on immiscible displacement in a microfluidic porous media. *Energies*, **12**(4): 664. doi:10.3390/en12040664.

Bachu S. 2015. Review of CO_2 storage efficiency in deep saline aquifers. *International Journal of Greenhouse Gas Control*, **40**: 188 - 202. doi:10.1016/j.ijggc.2015.01.007.

Battat S, Weitz DA, Whitesides GM. 2022. An outlook on microfluidics: the promise and the challenge. *Lab on a Chip*, **22**(3): 530 - 536. doi:10.1039/D1LC00731A.

Batz NG, Mellors JS, Alarie JP, et al. 2014. Chemical vapor deposition of aminopropyl silanes in microfluidic channels for highly efficient microchip capillary electrophoresis-electrospray ionization-mass spectrometry. *Analytical Chemistry*, **86**(7): 3493–3500. doi:10.1021/ac404106u.

Baumann G, Henninges J, De Lucia M. 2014. Monitoring of saturation changes and salt precipitation during CO_2 injection using pulsed neutron-gamma logging at the Ketzin pilot site. *International Journal of Greenhouse Gas Control*, **28**: 134–146. doi:10.1016/j.ijggc.2014.06.023.

Bohnsack D, Potten M, Freitag S, et al. 2021. Stress sensitivity of porosity and permeability under varying hydrostatic stress conditions for different carbonate rock types of the geothermal Malm reservoir in Southern Germany. *Geothermal Energy*, **9**(1): 15. doi:10.1186/s40517-021-00197-w.

Cai B, Li Q, Zhang X. 2021. China Carbon Dioxide Capture, Utilization and Storage (CCUS) Annual Report (2021) - China CCUS Pathway Research. Ministry of Ecology and Environment, Institute of Environmental Planning, Chinese Academy of Sciences, Wuhan Institute of Geotechnical Mechanics, China Agenda 21 Management Center.

Cai J, Jiao X, Wang H, et al. 2024. Multiphase fluid-rock interactions and flow behaviors in shale nanopores: A comprehensive review. *Earth-Science Reviews*, **104884**. doi:10.1016/j.earscirev.2024.104884.

Chen K, Liu P, Wang W, et al. 2023. Effects of capillary and viscous forces on two - phase fluid displacement in the microfluidic model. *Energy & Fuels*, **37**(22): 17263 - 17276. doi:10.1021/acs.energyfuels.3c03170.

Chen XS, Hu R, Zhou CX, et al. 2024. Capillary-driven backflow during salt precipitation in a rough fracture. *Water Resources Research*, **60**(3): e2023WR035451. doi:10.1029/2023WR035451.

Cheng C, Busch B, Hilgers C. 2023. A microfluidic study into salt precipitation in saline aquifers induced by continuous CO_2 injection. 84th EAGE Annual Conference and Exhibition, European Association of Geoscientists and Engineers, **2023**(1): 1 - 5. doi:10.3997/2214 - 4609.2023101505.

Chiquet P, Daridon JL, Broseta D, et al. 2007. CO_2 water interfacial tensions under pressure and temperature conditions of CO_2 geological storage. *Energy Conversion and Management*, **48**(3): 736 - 744. doi:10.1016/j.enconman.2006.09.011.

Civan F. 2023. *Reservoir Formation Damage: Fundamentals, Modeling, Assessment, and Mitigation*. Gulf Professional Publishing.

Cui G, Hu Z, Ning F, et al. 2023. A review of salt precipitation during CO_2 injection into saline aquifers and its potential impact on carbon sequestration projects in China. *Fuel*, **334**: 126615. doi:10.1016/j.fuel.2022.126615.

Da Wang Y, Kearney LM, Blunt MJ, et al. 2024. In situ characterization of heterogeneous surface wetting in porous materials. *Advances in Colloid and Interface Science*, **103122**. doi:10.1016/j.cis.2024.103122.

Darkwah-Owusu V, Md Yusof MA, Sokama-Neuyam YA, et al. 2024. Assessment of Advanced Remediation Tech-

niques for Enhanced CO_2 Injectivity: Laboratory Investigations and Implications for Improved CO_2 Flow in Saline Aquifers. *Energy & Fuels*, **38**(10): 8895–8908. doi:10.1021/acs.energyfuels.4c00949.

Dashtian H, Shokri N, Sahimi M. 2018. Pore - network model of evaporation - induced salt precipitation in porous media: The effect of correlations and heterogeneity. *Advances in water resources*, **112**: 59 - 71. doi:10.1016/j.advwatres.2017.12.004.

Dabrowski KM, Nooraiepour M, Masoudi M, et al. 2024. How does surface wettability alter salt precipitation and growth dynamics during CO_2 injection into saline aquifers: A microfluidic analysis. arXiv preprint arXiv, **2410**: 04910. doi:10.48550/arXiv.2410.04910.

Dabrowski KM, Nooraiepour M, Masoudi M, et al. 2025. Surface wettability governs brine evaporation and salt precipitation during carbon sequestration in saline aquifers: Microfluidic insights. *Science of The Total Environment*, **958**: 178110. doi:10.1016/j.scitotenv.2024.178110.

Dong L, Xiong Y, Huang Q, et al. 2021. Evaporation-induced salt crystallization and feedback on hydrological functions in porous media with different grain morphologies. *Journal of Hydrology*, **598**: 126427. doi:10.1016/j.jhydrol.2021.126427.

Dong L, Liu S, Huang G, et al. 2024. Evaporation with Salt Crystallization in Capillaries of Different Cross Sections. *Transport in Porous Media*, **151**(10): 2057 - 2079. doi:10.1007/s11242 - 024 - 02106 - 8.

Elsayed M, Isah A, Hib M, et al. 2022. A review on the applications of nuclear magnetic resonance (NMR) in the oil and gas industry: laboratory and field-scale measurements. *Journal of Petroleum Exploration and Production Technology*, **12**(10): 2747–2784. doi:10.1007/s13202-022-01476-3.

Galloway JM, Aslam ZP, Yeandel SR, et al. 2023. Electron transparent nanotubes reveal crystallization pathways in confinement. *Chemical Science*, **14**(24): 6705–6715. doi:10.1039/d3sc00869j.

Gao Y, Raeini AQ, Selem AM, et al. 2020. Pore-scale imaging with measurement of relative permeability and capillary pressure on the same reservoir sandstone sample under water-wet and mixed-wet conditions. *Advances in Water Resources*, **146**: 103786. doi:10.1016/j.advwatres.2020.103786.

Gogoi S, Gogoi SB. 2019. Review on microfluidic studies for EOR application. *Journal of Petroleum Exploration and Production Technology*, **9**: 2263 - 2277. doi:10.1007/s13202-019-0610-4.

Grude S, Landrø M, Dvorkin J. 2014. Pressure effects caused by CO_2 injection in the Tubåen Fm., the Snøhvit field. *International Journal of Greenhouse Gas Control*, **27**: 178–187. doi:10.1016/j.ijggc.2014.05.013.

Guggenheim EA. 1937. The theoretical basis of Raoult's law. *Transactions of the Faraday Society*, **33**: 151 - 156. doi:10.1039/TF9373300151.

Hao Y, Li Z, Su Y, et al. 2022. Experimental investigation of CO_2 storage and oil production of different CO_2 injection methods at pore - scale and core - scale. *Energy*, **254**: 124349. doi:10.1016/j.energy.2022.124349.

He D, Jiang P, Lun Z, et al. 2019. Pore scale CFD simulation of supercritical carbon dioxide drainage process in porous media saturated with water. *Energy Sources, Part A: Recovery, Utilization, and Environmental Effects*, **41**(15): 1791 - 1799. doi:10.1080/15567036.2018.1549155.

He D, Jiang P, Xu R. 2019. Pore-scale experimental investigation of the effect of supercritical CO_2 injection rate and surface wettability on salt precipitation. *Environmental Science & Technology*, **53**(24): 14744–14751. doi:10.1021/acs.est.9b03323.

He D, Xu R, Ji T, et al. 2022. Experimental investigation of the mechanism of salt precipitation in the fracture during CO_2 geological sequestration. *International Journal of Greenhouse Gas Control*, **118**: 103693. doi:10.1016/j.ijggc.2022.103693.

He D, Jiang P, Xu R. 2023. The influence of heterogeneous structure on salt precipitation during CO_2 geological storage. *Advances in Geo - Energy Research*, **7**(3): 189 - 198. doi:10.46690/ager.v7i3.261.

He D, Wang Z, Yuan H, et al. 2024. Experimental investigation of salt precipitation behavior and its impact on injectivity under variable injection operating conditions. *Journal of Natural Gas Science and Engineering*, **121**: 205198. doi:10.1016/j.jgsce.2023.205198.

Hiller T, Ardevol-Murison J, Muggeridge A, et al. 2019. The impact of wetting-heterogeneity distribution on capillary pressure and macroscopic measures of wettability. *SPE Journal*, **24**(01): 200–214. doi:10.2118/194191-PA.

Ho THM, Tsai PA. 2020. Microfluidic salt precipitation: implications for geological CO_2 storage. *Lab on a Chip*, **20**(20): 3806 - 3814. doi:10.1039/D0LC00238K.

Holtzman R, Segre E. 2015. Wettability stabilizes fluid invasion into porous media via nonlocal, cooperative pore filling. *Physical Review Letters*, **115**(16): 164501. doi:10.1103/PhysRevLett.115.164501.

Holtzman R. 2016. Effects of pore - scale disorder on fluid displacement in partially - wettable porous media. *Scientific Reports*, **6**(1): 36221. doi:10.1038/srep36221.

Hossain A, Rajput P, Li Z, et al. 2024. Engineering bioinspired microfluidics; biomimetic self - healing/cleaning coating designs and unique advanced materials. *Chemical Engineering Journal*, : 151336. doi:10.1016/j.cej.2024.151336.

Hu R, Wan J, Yang Z, et al. 2018. Wettability and flow rate impacts on immiscible displacement: A theoretical model. *Geophysical Research Letters*, **45**(7): 3077 - 3086. doi:10.1002/2017GL076600.

Hu X, Wang J, Zhang L, et al. 2022. Direct visualization of nanoscale salt precipitation and dissolution dynamics during CO_2 injection. *Energies*, **15**(24): 9567. doi:10.3390/en15249567.

Hwang J, Cho YH, Park MS, et al. 2019. Microchannel fabrication on glass materials for microfluidic devices. *International Journal of Precision Engineering and Manufacturing*, **20**: 479 - 495. doi:10.1007/s12541-019-00103-2.

Irannezhad A, Primkulov BK, Juanes R, et al. 2023. Fluid-fluid displacement in mixed-wet porous media. *Physical Review Fluids*, **8**(1): L012301. doi:10.1103/PhysRevFluids.8.L012301.

Iyer V, Issadore D, Aflatouni F. 2023. The next generation of hybrid microfluidic/integrated circuit chips: recent and upcoming advances in high-speed, high-throughput, and multifunctional lab-on-IC systems. *Lab on a Chip*, **23**(11): 2553–2576. doi:10.1039/D2LC01163H.

Jahanbakhsh A, Wlodarczyk KL, Hand DP, et al. 2020. Review of microfluidic devices and imaging techniques for fluid flow study in porous geomaterials. *Sensors*, **20**(14): 4030. doi:10.3390/s20144030.

Jannesarahmadi S, Aminzadeh M, Helmig R, et al. 2024. Quantifying salt crystallization impact on evaporation dynamics from porous surfaces. *Geophysical Research Letters*, **51**(22): e2024GL111080. doi:10.1029/2024GL111080.

Jeddizahed J, Rostami B. 2016. Experimental investigation of injectivity alteration due to salt precipitation during CO_2

sequestration in saline aquifers. *Advances in water resources*, **96**: 23 - 33. doi:10.1016/j.advwatres.2016.06.014.

Jeong GS, Lee J, Ki S, et al. 2017. Effects of viscosity ratio, interfacial tension and flow rate on hysteric relative permeability of CO_2/brine systems. *Energy*, **133**: 62 - 69. doi:10.1016/j.energy.2017.05.138.

Juska VB, Maxwell G, Estrela P, et al. 2023. Silicon microfabrication technologies for biology integrated advance devices and interfaces. *Biosensors and Bioelectronics*, **237**: 115503. doi:10.1016/j.bios.2023.115503.

Jung M, Brinkmann M, Seemann R, et al. 2016. Wettability controls slow immiscible displacement through local interfacial instabilities. *Physical Review Fluids*, **1**(7): 074202. doi:10.1103/PhysRevFluids.1.074202.

Kalde A, Lippold S, Loelsberg J, et al. 2022. Surface Charge Affecting Fluid–Fluid Displacement at Pore Scale. *Advanced Materials Interfaces*, **9**(9): 2101895. doi:10.1002/admi.202101895.

Kalde AM, Grosseheide M, Brosch S, et al. 2022. Micromodel of a Gas Diffusion Electrode Tracks In - Operando Pore - Scale Wetting Phenomena. *Small*, **18**(49): 2204012. doi:10.1002/smll.202204012.

Kang C, Mirbod P. 2019. Porosity effects in laminar fluid flow near permeable surfaces. *Physical Review E*, **100**(1): 013109. doi:10.1103/PhysRevE.100.013109.

Kim J, Ferrari A, Ewy R, et al. 2025. Water retention behavior of a gas shale: Wettability-controlled water saturation and anisotropic hydromechanical response. *International Journal of Rock Mechanics and Mining Sciences*, **188**: 106061. doi:10.1016/j.ijrmms.2025.106061.

Kim M, Sell A, Sinton D. 2013. Aquifer - on - a - Chip: understanding porescale salt precipitation dynamics during CO_2 sequestration. *Lab on a Chip*, **13**(13): 2508 - 2518. doi:10.1039/C3LC00031A.

Kumar R, Campbell S, Sonnenthal E, et al. 2020. Effect of brine salinity on the geological sequestration of CO_2 in a deep saline carbonate formation. *Greenhouse Gases: Science and Technology*, **10**(2): 296–312. doi:10.1002/ghg.1960.

Kuzin A, Panda K, Chernyshev V, et al. 2024. Microfluidic–nanophotonic sensor for on-chip analysis of complex refractive index. *Applied Physics Letters*, **124**(6): 063701. doi:10.1063/5.0190351.

Lake JR, Heyde KC, Ruder WC. 2017. Low-cost feedback-controlled syringe pressure pumps for microfluidics applications. *PLoS One*, **12**(4): e0175089. doi:10.1371/journal.pone.0175089.

Lei W, Gong W, Lu X, et al. 2024. Fluid entrapment during forced imbibition in a multidepth microfluidic chip with complex porous geometry. *Journal of Fluid Mechanics*, **987**: A3. doi:10.1017/jfm.2024.358.

Lei W, Lu X, Gong W, et al. 2023. Triggering interfacial instabilities during forced imbibition by adjusting the aspect ratio in depth - variable microfluidic porous media. *Proceedings of the National Academy of Sciences*, **120**(50): e2310584120. doi:10.1073/pnas.2310584120.

Lei W, Lu X, Wang M. 2023. Multiphase displacement manipulated by micro/nanoparticle suspensions in porous media via microfluidic experiments: From interface science to multiphase flow patterns. *Advances in Colloid and Interface Science*, **311**: 102826. doi:10.1016/j.cis.2022.102826.

Lenormand R, Touboul E, Zarcone C. 1988. Numerical models and experiments on immiscible displacements in porous media. *Journal of Fluid Mechanics*, **189**: 165 - 187. doi:10.1017/S0022112088000953.

Leung DYC, Caramanna G, Maroto-Valer MM. 2014. An overview of current status of carbon dioxide capture and storage technologies. *Renewable and Sustainable Energy Reviews*, **39**: 426–443. doi:10.1016/j.rser.2014.07.093.

Li B, Zhou J, Gan Q, et al. 2024. CO_2 Sequestration: Influence on Mineral Dynamics and Reservoir Permeability in Depleted Carbonates. *Energy & Fuels*, **38**(24): 23600 - 23615. doi:10.1021/acs.energyfuels.4c04618.

Li JX, Rezaee R, Müller TM, et al. 2021. Pore size distribution controls dynamic permeability. *Geophysical Research Letters*, **48**(5): e2020GL090558. doi:10.1029/2020GL090558.

Li L, Zhang D, Su Y, et al. 2024. Microfluidic insights into CO_2 sequestration and enhanced oil recovery in laminated shale reservoirs: Postfracturing interface dynamics and micro-scale mechanisms. *Advances in Geo-Energy Research*, **13**(3): 203–217. doi:10.46690/ager.v13i3.395.

Li X, Mao X, Li X, et al. 2024. A one - step process for multi - gradient wettability modification on a polymer surface. *Analyst*, **149**(7): 2103 - 2113. doi:10.1039/D3AN02185H.

Li X, Peng B, Liu Q, et al. 2023. Micro and nanobubbles technologies as a new horizon for CO_2-EOR and CO_2 geological storage techniques: A review. *Fuel*, **341**: 127661. doi:10.1016/j.fuel.2023.127661.

Li Y, Blois G, Kazemifar F, et al. 2019. High - speed quantification of pore - scale multiphase flow of water and supercritical CO_2 in 2-D heterogeneous porous micromodels: Flow regimes and interface dynamics. *Water Resources Research*, **55**(5): 3758 - 3779. doi:10.1029/2018WR024635.

Liefferink RW, Naillon A, Bonn D, et al. 2018. Single layer porous media with entrapped minerals for microscale studies of multiphase flow. *Lab on a Chip*, **18**(7): 1094 - 1104. doi:10.1039/C7LC01377A.

Liu H, He Q, Borgia A, et al. 2016. Thermodynamic analysis of a compressed carbon dioxide energy storage system using two saline aquifers at different depths as storage reservoirs. *Energy Conversion and Management*, **127**: 149–159. doi:10.1016/j.enconman.2016.08.096.

Liu Y, Lv P, Liu Y, et al. 2016. CO_2/water two - phase flow in a two dimensional micromodel of heterogeneous pores and throats. *RSC Advances*, **6**(77): 73897 - 73905. doi:10.1039/C6RA10229H.

Liu Y, Su G, Wang W, et al. 2024. A novel multifunctional SERS microfluidic sensor based on ZnO/Ag nanoflower arrays for label - free ultrasensitive detection of bacteria. *Analytical Methods*, **16**(14): 2085 - 2092. doi:10.1039/D4AY00018H.

Lönartz MI, Yang Y, Deissmann G, et al. 2023. Capturing the dynamic processes of porosity clogging. *Water Resources Research*, **59**(11): e2023WR034722. doi:10.1029/2023WR034722.

Lopez O, Youssef S, Estublier A, et al. 2020. Permeability alteration by salt precipitation: numerical and experimental investigation using X-Ray Radiography. *E3S Web of Conferences*, **146**: 03001. doi:10.1051/e3sconf/202014603001.

Lu X, Kharaghani A, Adloo H, et al. 2020. The Brooks and Corey capillary pressure model revisited from pore network simulations of capillarity controlled invasion percolation process. *Processes*, **8**(10): 1318. doi:10.3390/pr8101318.

Maes J, Geiger S. 2018. Direct pore-scale reactive transport modelling of dynamic wettability changes induced by surface complexation. *Advances in Water Resources*, **111**: 6–19. doi:10.1016/j.advwatres.2017.10.032.

Massimiani A, Panini F, Marasso SL, et al. 2023. Design, fabrication, and experimental validation of microfluidic devices for the investigation of pore-scale phenomena in underground gas storage systems. *Micromachines*, **14**(2): 308.

doi:10.3390/mi14020308.
Mascle M, Lopez O, Deschamps H, et al. 2023. Investigation of salt precipitation dynamic in porous media by X - ray and Neutron dual - modality imaging. *Science and Technology for Energy Transition*, **78**: 11. doi:10.2516/stet/2023009.
Mascini A, Boone M, Van Offenwert S, et al. 2021. Fluid invasion dynamics in porous media with complex wettability and connectivity. *Geophysical Research Letters*, **48**(22): e2021GL095185. doi:10.1029/2021GL095185.
Miri R, van Noort R, Aagaard P, et al. 2015. New insights on the physics of salt precipitation during injection of CO_2 into saline aquifers. *International Journal of Greenhouse Gas Control*, **43**: 10–21. doi:10.1016/j.ijggc.2015.10.004.
Mouli-Castillo J, Wilkinson M, Mignard D, et al. 2019. Inter-seasonal compressed-air energy storage using saline aquifers. *Nature Energy*, **4**(2): 131–139. doi:10.1038/s41560-018-0311-0.
Mu X, Chen FD, Dang KM, et al. 2023. Implantable photonic neural probes with 3D - printed microfluidics and applications to uncaging. *Frontiers in Neuroscience*, **17**: 1213265. doi:10.3389/fnins.2023.1213265.
Naillon A, Joseph P, Prat M. 2017. Sodium chloride precipitation reaction coefficient from crystallization experiment in a microfluidic device. *Journal of Crystal Growth*, **463**: 201–210. doi:10.1016/j.jcrysgro.2017.01.058.
Nordbotten JM, Celia MA, Bachu S. 2005. Injection and storage of CO_2 in deep saline aquifers: analytical solution for CO_2 plume evolution during injection. *Transport in Porous media*, **58**: 339 - 360. doi:10.1007/s11242 - 004 - 0670 - 9.
Noiriel C, Steefel CI, Yang L, et al. 2016. Effects of pore - scale precipitation on permeability and flow. *Advances in Water Resources*, **95**: 125 - 137. doi:10.1016/j.advwatres.2015.11.013.
Nooraiepour M, Fazeli H, Miri R, et al. 2018. Effect of CO_2 phase states and flow rate on salt precipitation in shale caprocks—a microfluidic study. *Environmental Science & Technology*, **52**(10): 6050 - 6060. doi:10.1021/acs.est.8b00251.
Nooraiepour M, Masoudi M, Shokri N, et al. 2021. Probabilistic nucleation and crystal growth in porous medium: new insights from calcium carbonate precipitation on primary and secondary substrates. *ACS omega*, **6**(42): 28072 - 28083. doi:10.1021/acsomega.1c04147.
Norouzi AM, Babaei M, Han WS, et al. 2021. CO_2 - plume geothermal processes: A parametric study of salt precipitation influenced by capillary driven backflow. *Chemical Engineering Journal*, **425**: 130031. doi:10.1016/j.cej.2021.130031.
Ott H, Roels SM, De Kloe K. 2015. Salt precipitation due to supercritical gas injection: I. Capillary - driven flow in unimodal sandstone. *International Journal of Greenhouse Gas Control*, **43**: 247 - 255. doi:10.1016/j.ijggc.2015.01.005.
Parvin S, Masoudi M, Sundal A, et al. 2020. Continuum scale modelling of salt precipitation in the context of CO_2 storage in saline aquifers with MRST compositional. *International Journal of Greenhouse Gas Control*, **99**: 103075. doi:10.1016/j.ijggc.2020.103075.
Patil VV, McPherson BJ. 2020. Identifying Hydrogeochemical Conditions for Fault Self-Sealing in Geological Storage. *Water Resources Research*, **56**(3): e2018WR024436. doi:10.1029/2018WR024436.
Peysson Y, André L, Azaroual M. 2014. Well injectivity during CO_2 storage operations in deep saline aquifers—Part 1: Experimental investigation of drying effects, salt precipitation and capillary forces. *International Journal of Greenhouse Gas Control*, **22**: 291 - 300. doi:10.1016/j.ijggc.2013.10.031.
Pitzer KS, Peiper JC, Busey RH. 1984. Thermodynamic properties of aqueous sodium chloride solutions. *Journal of Physical and Chemical Reference Data*, **13**(1): 1 - 102. doi:10.1063/1.555709.
Qi ZB, Xu L, Xu Y, et al. 2018. Disposable silicon-glass microfluidic devices: precise, robust and cheap. *Lab on a Chip*, **18**(24): 3872–3880. doi:10.1039/C8LC01109E.
Qian C, Rui Z, Liu Y, et al. 2025. Microfluidic investigation on microscopic flow and displacement behavior of CO_2 multiphase system for CCUSEOR in heterogeneous porous media. *Chemical Engineering Journal*, **505**: 159135. doi:10.1016/j.cej.2024.159135.
Rabbani HS, Or D, Liu Y, et al. 2018. Suppressing viscous fingering in structured porous media. *Proceedings of the National Academy of Sciences*, **115**(19): 4833 - 4838. doi:10.1073/pnas.1800729115.
Ran B, Omikrine - Metalssi O, Fen - Chong T, et al. 2023. Pore crystallization and expansion of cement pastes in sulfate solutions with and without chlorides. *Cement and Concrete Research*, **166**: 107099. doi:10.1016/j.cemconres.2023.107099.
Rasmusson K, Rasmusson M, Tsang Y, et al. 2016. A simulation study of the effect of trapping model, geological heterogeneity and injection strategies on CO_2 trapping. *International Journal of Greenhouse Gas Control*, **52**: 52 - 72. doi:10.1016/j.ijggc.2016.06.020.
Rathnaweera TD, Ranjith PG, Perera MSA, et al. 2016. Influence of CO_2–brine co-injection on CO_2 storage capacity enhancement in deep saline aquifers: an experimental study on Hawkesbury sandstone formation. *Energy & Fuels*, **30**(5): 4229–4243. doi:10.1021/acs.energyfuels.6b00113.
Ren J, Wang Y, Feng D, et al. 2021. CO_2 migration and distribution in multiscale-heterogeneous deep saline aquifers. *Advances in Geo-Energy Research*, **5**(3): 333–346. doi:10.46690/ager.v5i3.171.
Ren J, Wang Y, Zhang Y. 2018. A numerical simulation of a dry-out process for CO_2 sequestration in heterogeneous deep saline aquifers. *Greenhouse Gases: Science and Technology*, **8**(6): 1090–1109. doi:10.1002/ghg.1821.
Ren J, Wang Y, Feng D, et al. 2022. Characterization method and application of heterogeneous reservoir based on different data quantity. *Lithosphere*, **2021**(4): 8267559. doi:10.2113/2022/8267559.
Roosta A, Zendehboudi S, Rezaei N. 2024. Improving the estimation accuracy of confined vapor–liquid equilibria by fine-tuning the pure component parameter in the PC-SAFT equation of state. *Physical Chemistry Chemical Physics*, **26**(18): 13790–13803. doi:10.1039/D3CP05979K.
Rufai A, Crawshaw J. 2017. Micromodel observations of evaporative drying and salt deposition in porous media. *Physics of Fluids*, **29**(12): 126603. doi:10.1063/1.5004246.
Rufai A, Crawshaw J. 2018. Effect of wettability changes on evaporation rate and the permeability impairment due to salt deposition. *ACS Earth and Space Chemistry*, **2**(4): 320 - 329. doi:10.1021/acsearthspacechem.7b00126.
Scherer GW. 1999. Crystallization in pores. *Cement and Concrete Research*, **29**(8): 1347–1358. doi:10.1016/S0008-8846(99)00002-2.
Schneider MH, Willaime H, Tran Y, et al. 2010. Wettability patterning by UV - initiated graft polymerization of poly (acrylic acid) in closed microfluidic systems of complex geometry. *Analytical Chemistry*, **82**(21): 8848 - 8855. doi:10.1021/ac101345m.
Scanziani A, Lin Q, Alhosani A, et al. 2020. Dynamics of fluid displacement in mixed-wet porous media. *Pro-*

ceedings of the Royal Society A, **476**(2240): 20200040. doi:10.1098/rspa.2020.0040.

Seo S, Mastiani M, Hafez M, et al. 2019. Injection of in - situ generated CO_2 microbubbles into deep saline aquifers for enhanced carbon sequestration. *International Journal of Greenhouse Gas Control*, **83**: 256 - 264. doi:10.1016/j.ijggc.2019.02.017.

Shao J, You L, Jia N, et al. 2025. Real - time visualization of salt crystallization in 2 - D microchannels. *Geoenergy Science and Engineering*, **246**: 213622. doi:10.1016/j.geoen.2024.213622.

Sibiryakov B, Leite LWB, Sibiriakov E. 2021. Porosity, specific surface area and permeability in porous media. *Journal of Applied Geophysics*, **186**: 104261. doi:10.1016/j.jappgeo.2021.104261.

Silverio V, Canane PAG, Cardoso S. 2019. Surface wettability and stability of chemically modified silicon, glass and polymeric surfaces via room temperature chemical vapor deposition. *Colloids and Surfaces A: Physicochemical and Engineering Aspects*, **570**: 210 - 217. doi:10.1016/j.colsurfa.2019.03.032.

Skottvoll FS, Escobedo - Cousin E, Mielnik MM. 2024. The Role of Silicon Technology in Organ - On - Chip: Current Status and Future Perspective. *Advanced Materials Technologies*, 2401254. doi:10.1002/admt.202401254.

Smith N, Boone P, Oguntimehin A, et al. 2022. Quest CCS facility: Halite damage and injectivity remediation in CO_2 injection wells. *International Journal of Greenhouse Gas Control*, **119**: 103718. doi:10.1016/j.ijggc.2022.103718.

Suo S, O'Kiely D, Liu M, et al. 2024. Geometry effects on interfacial dynamics of gas - driven drainage in a gradient capillary. *Water Resources Research*, **60**(9): e2023WR036766. doi:10.1029/2023WR036766.

Sun W, Li J, Liu Q, et al. 2024. Complexity upgrade and triggering mechanism of mixed-wettability: Comparative study of CO_2 displacement in different phases. *Fuel*, **369**: 131798. doi:10.1016/j.fuel.2024.131798.

Sun Y, Yu H, Yang B. 2024. Impact of Wettability on CO_2 Dynamic Dissolution in Three - Dimensional Porous Media: Pore - Scale Simulation Using the Lattice Boltzmann Method. *Langmuir*, **40**(43): 22658 - 22672. doi:10.1021/acs.langmuir.4c02412.

Sun Z, Santamarina JC. 2019. Haines jumps: Pore scale mechanisms. *Physical Review E*, **100**(2): 023115. doi:10.1103/PhysRevE.100.023115.

Tang Y, Yang R, Du Z, et al. 2015. Experimental study of formation damage caused by complete water vaporization and salt precipitation in sandstone reservoirs. *Transport in Porous Media*, **107**: 205 - 218. doi:10.1007/s11242-014-0433-1.

Wang B. 2016. *Study on the evaporation and salt deposition patterns of high salinity formation water in the near wellbore area of gas fields*. Chengdu: Southwest Petroleum University, China.

Wang B, Wang X, Liang Q, et al. 2024. Investigation of pore - Scale evaporative drying, salt precipitation and crystallization migration in CO_2 injection process by a Lab - on - a - Chip system. SPE Canadian Energy Technology Conference, SPE, D011S005R002. doi:10.2118/218048 - MS.

Wang W, Chang S, Gizzatov A. 2017. Toward reservoir-on-a-chip: fabricating reservoir micromodels by in situ growing calcium carbonate nanocrystals in microfluidic channels. *ACS Applied Materials & Interfaces*, **9**(34): 29380–29386. doi:10.1021/acsami.7b10746.

Wang Y, Liu Y. 2014. Dry-out effect and site selection for CO_2 storage in deep saline aquifers. *Rock and Soil Mechanics*, **35**(6): 1711–1717.

Wang Y, Mackie E, Rohan J, et al. 2009. Experimental study on halite precipitation during CO_2 sequestration. Paper S-CA2009 - 25 Presented at International Symposium of the Society of Core Analysts, Noordwijk, The Netherlands, 27 - 30.

Wang Z, Zheng H, Xia H. 2011. Femtosecond laser - induced modification of surface wettability of PMMA for fluid separation in microchannels. *Microfluidics and Nanofluidics*, **10**: 225 - 229. doi:10.1007/s10404 - 010 - 0662 - 8.

Wang Z, Pereira JM, Gan Y. 2021. Effect of grain shape on quasi - static fluid - fluid displacement in porous media. *Water Resources Research*, **57**(4): e2020WR029415. doi:10.1029/2020WR029415.

Wang Z, Ong LJY, Gan Y, et al. 2024. PoroFluidics: deterministic fluid control in porous microfluidics. *Lab on a Chip*, **24**(17): 4050 - 4059. doi:10.1039/D4LC00518J.

Wang Z, Chen S, Yuan H, et al. 2023. Experimental Investigation on Salt Precipitation Behavior during Carbon Geological Sequestration: Considering the Influence of Formation Boundary Solutions. *Energy & Fuels*, **38**(1): 514 - 525. doi:10.1021/acs.energyfuels.3c03767.

Wei G, Hu R, Liao Z, et al. 2021. Effect of wettability on displacement efficiency of two - phase flow in porous media. *Chinese Journal of Theoretical and Applied Mechanics*, **53**(4): 1008 - 1017.

Wei H, Sha X, Chen L, et al. 2024. Visualization of Multiphase Reactive Flow and Mass Transfer in Functionalized Microfluidic Porous Media. *Small*, 2401393. doi:10.1002/smll.202401393.

Wei YM, Chen K, Kang JN, et al. 2022. Policy and management of carbon peaking and carbon neutrality: A literature review. *Engineering*, **14**: 52–63. doi:10.1016/j.eng.2021.12.018.

Wu R, Chen F. 2023. Interplay between salt precipitation, corner liquid film flow, and gas–liquid displacement during evaporation in microfluidic pore networks. *Journal of Applied Physics*, **133**: 074701. doi:10.1063/5.0135135.

Wu Y, Chen Y, Cheng Y. 2024. Building an Arduino-Based Open-Source Programmable Multichannel Syringe Pump: A Useful Tool for Fluid Delivery in Microfluidics and Flow Chemistry. *Journal of Chemical Education*, **101**(5): 1951–1958. doi:10.1021/acs.jchemed.4c00033.

Xing X, Ou Yang J, Zhou L, et al. 2022. Advances in crystallization research in restricted spaces. *Chemical Industry and Engineering*, **39**(5): 39–48.

Yan L, Niftaliyev R, Voskov D, et al. 2025. Dynamics of salt precipitation at pore scale during CO_2 subsurface storage in saline aquifer. *Journal of Colloid and Interface Science*, **678**: 419–430. doi:10.1016/j.jcis.2024.08.265.

Yang F, Guan D, Starchenko V, et al. 2024. Effect of nucleation heterogeneity on mineral precipitation in confined environments. *Geophysical Research Letters*, **51**(9): e2023GL107185. doi:10.1029/2023GL107185.

Yang Z, Méheust Y, Neuweiler I, et al. 2019. Modeling immiscible two - phase flow in rough fractures from capillary to viscous fingering. *Water Resources Research*, **55**(3): 2033 - 2056. doi:10.1029/2018WR024045.

Zhang C, Oostrom M, Wietsma TW, et al. 2011. Influence of viscous and capillary forces on immiscible fluid displacement: Pore - scale experimental study in a water - wet micromodel demonstrating viscous and capillary fingering. *Energy & Fuels*, **25**(8): 3493 - 3505. doi:10.1021/ef101732k.

Zhang H, Sun Z, Zhang N, et al. 2024. Brine drying and salt precipitation in porous media: A microfluidics study. *Water Resources Research*, **60**(1): e2023WR035670.

doi:10.1029/2023WR035670.

Zhang L, Lai F, Meng Y, et al. 2025. Classification evaluation of the suitability of CO_2 storage in Saline Aquifers. *Geoenergy Science and Engineering*, **249**: 213796. doi:10.1016/j.geoen.2025.213796.

Zhang Q, Kuang G, Wang L, et al. 2024. Tailoring drug delivery systems by microfluidics for tumor therapy. *Materials Today*, **73**: 151 - 178. doi:10.1016/j.mattod.2024.01.004.

Zhang W, Gu X, Zhong W, et al. 2022. Review of transparent soil model testing technique for underground construction: Ground visualization and result digitalization. *Underground Space*, **7**(4): 702–723. doi:10.1016/j.undsp.2020.05.003.

Zhao B, MacMinn CW, Juanes R. 2016. Wettability control on multiphase flow in patterned microfluidics. *Proceedings of the National Academy of Sciences*, **113**(37): 10251 - 10256. doi:10.1073/pnas.1603387113.

Zhou CX, Hu R, Li HW, et al. 2022. Pore-scale visualization and quantification of dissolution in microfluidic rough channels. *Water Resources Research*, **58**(11): e2022WR032255. doi:10.1029/2022WR032255.

Zhou Y, Liao XW, Zhang XL, et al. 2021. The effect of inorganic salt precipitation on oil recovery during CO_2 flooding: A case study of Chang 8 block in Changqing oilfield, NW China. *Petroleum Exploration and Development*, **48**(2): 442–449. doi:10.1016/S1876-3804(21)60035-6.

Zhu Y, Hu Y, Zhu Y. 2024. Can China's energy policies achieve the "dual carbon" goal? A multi-dimensional analysis based on policy text tools. *Environment, Development and Sustainability*, **2024**: 1–40. doi:10.1007/s10668-024-05190-4.

Zou S, Liu Y, Cai J, et al. 2020. Influence of capillarity on relative permeability in fractional flows. *Water Resources Research*, **56**(11): e2020WR027624. doi:10.1029/2020WR027624.

Zou S, Chen D, Kang N, et al. 2024. An experimental investigation on the energy signature associated with multiphase flow in porous media displacement regimes. *Water Resources Research*, **60**(3): e2023WR036241. doi:10.1029/2023WR036241.

Zuluaga E, Monsalve JC. 2003. Water vaporization in gas reservoirs. In SPE Eastern Regional Meeting, SPE, SPE - 84829 - MS. doi:10.2118/84829 - MS.

Zwanenburg EA, Williams MA, Warnett JM. 2021. Review of high-speed imaging with lab-based x-ray computed tomography. *Measurement Science and Technology*, **33**(1): 012003. doi:10.1088/1361-6501/ac354a.